Macromolecules

Article

pubs.acs.org/Macromolecules

The Copolymer Blending Method: A New Approach for Targeted Assembly of Micellar Nanoparticles

Daniel B. Wright,[†] Joseph P. Patterson,[§] Anaïs Pitto-Barry,[†] Annhelen Lu,[†] Nigel Kirby,[∥] Nathan C. Gianneschi,[§] Christophe Chassenieux,*[,‡] Olivier Colombani,*[,‡] and Rachel K. O'Reilly*[,†]

[†]Department of Chemistry, University of Warwick, Gibbet Hill Road, Coventry CV4 7AL, U.K.

[‡]Département PCI, Université du Maine, Avenue Olivier Messiaen, 72085 Le Mans, Cedex 09, France

[§]Department of Chemistry & Biochemistry, University of California, San Diego, 9500 Gilman Drive, La Jolla, California 92093, United States

[∥]Australian Synchrotron, 800 Blackburn Road, Clayton, Victoria 3168, Australia

Supporting Information

ABSTRACT: Polymer self-assembly in solution is a simple strategy for the preparation of elegant yet complex nanomaterials. However, exhaustive synthesis of the copolymer synthons is often required to access specific assemblies. In this work we show that the blending of just two diblock copolymers with identical block lengths but varying hydrophobic monomer incorporations can be used to access a range of assemblies of intermediate hydrophobic composition. Indeed, the nanostructures produced from blending are identical to those formed with the directly synthesized copolymer of the same composition. This new approach presents researchers with a more efficient and accessible methodology to access precision self-assembled nanostructures, and we highlight its potential by applying it to a demonstrator catalytically active system.

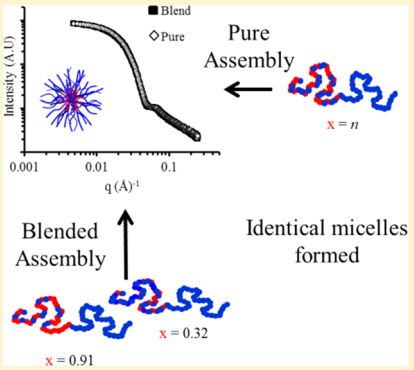

Nature captivates us with its ability to produce precise supramolecular nanostructures in highly competitive environments. In soft nanotechnology, attempts have been made to mimic the form and function of Nature's nanostructures using amphiphilic block copolymers which spontaneously self-assemble in selective solvents.[1−3] These synthetic nanostructures have enormous potential in a variety of applications including delivery agents, imaging, and enhanced oil recovery.[4−9] However, for an amphiphilic block copolymer to be specific to a desired application, the chemical structure must be adapted to yield the desired characteristics on the nanoscale in terms of size, aggregation number, functionality, and often response to an external stimulus.[10−12] This explains partly why a plethora of amphiphilic block copolymers and associated assembled nanostructures can be found in the literature, each new nanostructure requiring a new polymer and therefore a new synthetic batch.

To overcome this problem of laborious custom polymer synthesis for every desired nanostructure, an attractive strategy would be to blend two polymers, differing in terms of structural characteristics and stimuli response, to obtain a range of blends exhibiting characteristics between those of the two polymers.[13−21] This strategy would provide a route for accessing a wide range of functional properties or responses to stimuli, with only two polymers blended at various stoichiometry rather than a different polymer for each desired property.

Although previous reports exist on the blending of diblock copolymers, these reports have utilized blending to explore polymer morphologies that are typically not accessed through the self-assembly of a single polymer system.[22−24] In contrast here, our strategy was to blend two block−random diblock copolymers for a targeted assembly approach where specific polymer assemblies with precise characteristics could then be generated. Here the block−random diblock copolymers consist of a homopolymeric hydrophilic block connected to a hydrophobic block containing both hydrophilic and hydrophobic units statistically distributed.[25] The use of such polymers presents two assets. First, it has been shown recently that modifying the ratio of hydrophilic to hydrophobic units distributed statistically in the associating block allowed for tunable characteristics of the assemblies in water in terms of aggregation and resulting properties.[26−33] Moreover, incorporating hydrophilic units within the hydrophobic block of such polymers moderates their hydrophobicity so that the resulting self-assembled structures are in dynamic equilibrium with free unassembled chains (unimers).[27−30,33] It must be realized that this second aspect is a prerequisite of the utmost importance for the proposed targeted assembly strategy. Indeed, most amphiphilic block copolymers described in the literature lead to

Received: June 29, 2015
Revised: August 10, 2015
Published: August 31, 2015

DOI: 10.1021/acs.macromol.5b01426
Macromolecules 2015, 48, 6516−6522

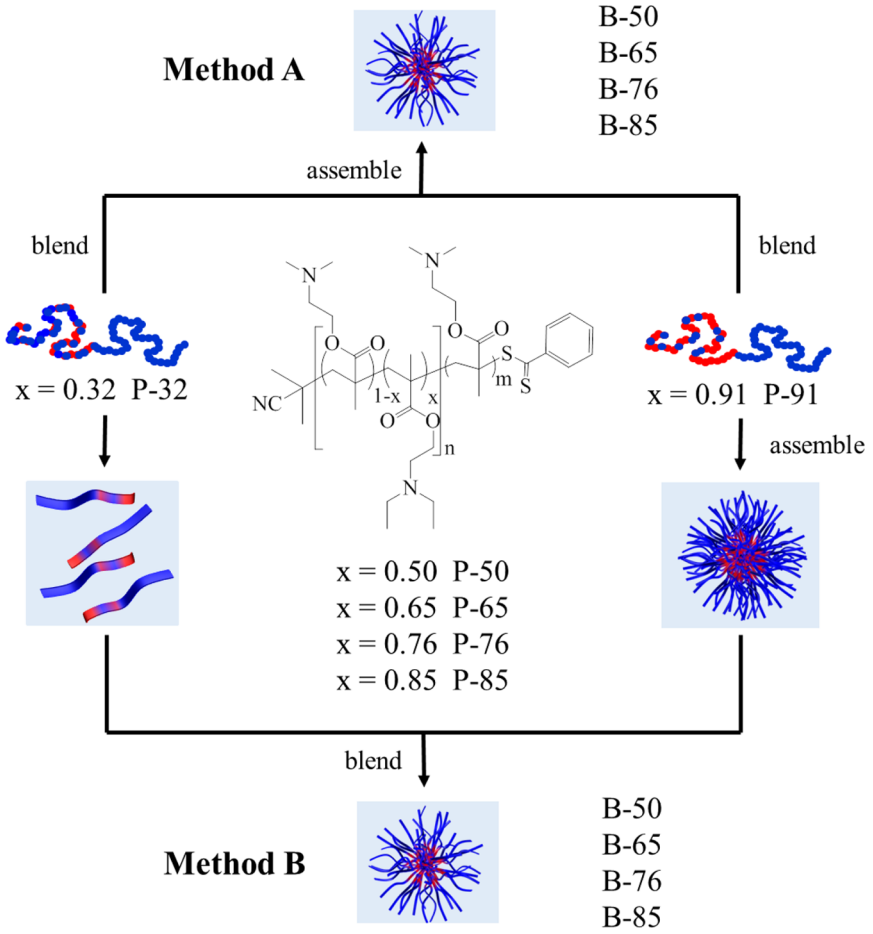

Figure 1. Schematic demonstrating the blending protocols employed. Center: schematic of the P(DMAEMA-*co*-DEAEMA)-*b*-PDMAEMA diblock copolymers. Method A: dry powder mixing (unimer blending); polymers are first mixed in the unimer state to match the desired DEAMEA *n* % and then subsequently assembled. Method B: micelle blending; polymers are first solubilized separately and then mixed to match the desired DEAEMA *n* %. Using method B, **P-91** is already assembled whereas **P-32** exists as unimers at $\alpha = 0$.

"frozen" self-assemblies.[34] Since these out-of-equilibrium structures are unable to reorganize, two micelles consisting of different polymers could not rearrange into mixed micelles. Indeed, even if the mixing was thermodynamically possible, it would be prevented for kinetic reasons.[16,18,20,24,34−38]

Our strategy consisted in mixing two block−random copolymers differing only in the ratio of comonomers in order to form blended micelles whose size and aggregation number depended on the content of each block−random copolymer in the blend. This simple blending protocol allows us to tune the characteristics of blended micelles in solution by simple formulation rather than by a demanding synthetic approach. Moreover, the blended micelles were structurally identical to those formed by a single block−random copolymer matching the overall composition of the blend. Given the simplicity of this method, we extended it to a catalytically active L-proline system, allowing us to specifically target precise and isolated catalytic pockets mimicking those found in natural biological systems.

RESULTS AND DISCUSSION

Formation of Blended Micelles. First, we studied the self-assembly in aqueous solution of blends of two P(DMAEMA-*co*-DEAEMA)-*b*-PDMAEMA diblock copolymers (DMAEMA: *N*,*N*-dimethylaminoethylmethacrylate, DEAEMA: *N*,*N*-diethylaminoethylmethacrylate) (Figure 1) containing respectively 32 mol% (**P-32**, where P stands for "pure") and 91 mol% (**P-91**) of DEAEMA in the core-forming block. Altering the ratio of these two polymers in the blend allowed us to target different DEAEMA contents (**B-50**, **B-65**, **B-76**, and **B-85**, where B stands for "blend"). The behavior of the blends could then be compared with that of pure P(DMAEMA-*co*-DEAEMA)-*b*-PDMAEMA polymers with the same average composition (**P-50**, **P-65**, **P-76**, and **P-85**), but where all chains are quasi-identical. The synthesis and characterization in aqueous solution of the pure diblock copolymers with varying DEAEMA incorporation were reported previously (Table 1).[33]

Here, all polymers were studied at $\alpha = 0$ in 0.1 M NaCl solution, and thus all DEAEMA units are hydrophobic. α represents the overall ionization degree of the DEAEMA and DMAEMA units; that is, the ratio of these units that are positively charged. Note that at $\alpha = 0$ **P-91** self-assembles into spherical micelles, whereas **P-32** remains as unimers. Two methods of preparation were used to verify if equilibrium was reached and that blended micelles were obtained by the coassembly of **P-91** and of **P-32** rather than a mixture of micelles of **P-91** and unimers of **P-32**. Method A (unimer blending, Figure 1) consisted of mixing bulk polymer powders and dissolving the polymers at $\alpha = 1$ and finally lowering the value of α to 0. With this method, the starting solution is a mixture of unimers, which probably favors the formation of blended micelles as thermodynamic equilibrium is reached

DOI: 10.1021/acs.macromol.5b01426
Macromolecules 2015, 48, 6516−6522

Table 1. Characteristics of the P(DMAEMA$_{1-x}$-*co*-DEAEMA$_x$)$_n$-*b*-PDMAEMA$_m$ Diblock Copolymers

diblock copolymer	x^a	n^b	m^b	$M_{n,NMR}{}^b$ (kDa)	$M_{n,SEC}{}^c$ (kDa)	$Đ_{SEC}{}^c$
P-32	0.32	35	30	10.7	13.8	1.16
P-50	0.50	34	32	11.1	13.4	1.18
P-65	0.65	36	35	12.3	14.2	1.12
P-76	0.76	25	34	10.0	12.8	1.18
P-85	0.85	31	35	11.4	13.9	1.17
P-91	0.91	28	32	10.4	13.5	1.10

[a]Determined by ^{1}H NMR spectroscopy using the signals at δ = 4.20 and 2.10 ppm. [b]Determined by end-group analysis from ^{1}H NMR spectroscopy. [c]From SEC based on poly(methyl methacrylate) standards and DMF as the eluent.

upon decrease of α, the solvent quality for the core-forming block.[39,40] For method B, (micelle blending, Figure 1), **P-32** and **P-91** are first dispersed independently and then blended only once they have reached α = 0. If unimer exchange does not occur, no blended micelles are expected to form due to kinetic limitations.

First, it can be seen in Figures 2a and 2b that steady state is only reached after several days with method B, the micelle blending route, whereas with method A blended micelles are formed after 1 day. However, both methods lead to the same structures being formed (Figure 2c), which is strongly indicative of both blend systems being at equilibrium. At equilibrium (final blend state), the weight-average aggregation number of the micelles is strongly different from the value expected for a mixture of nonblended **P-91** micelles and **P-32** unimers (shown as the straight line in Figure 2a) which can be calculated according to eq 1, where C is the weight concentration of the polymers in solution. It can be concluded that no matter the preparation method, **P-32** and **P-91** co-assemble at α = 0 into blended micelles where the structure is governed by the blending ratio of the two parent polymers.

$$N_{agg,mix} = \frac{C_{\mathbf{P\text{-}91}} N_{agg,\mathbf{P\text{-}91}} + C_{\mathbf{P\text{-}32}} N_{agg,\mathbf{P\text{-}32}}}{C_{\mathbf{P\text{-}91}} + C_{\mathbf{P\text{-}32}}} \quad (1)$$

Since blended micelles are formed even with method B and taking into account that these hybrid micelles are smaller in aggregation number than the initial **P-91** micelles, it can be deduced that unimer exchange does occur, causing the formation of the blended micelles.[41−43] It should be noted that for star-like micelles R_h only weakly depends on N_{agg}; hence, N_{agg} varied during the reorganization but R_h was hardly affected.[44] Additional small-angle X-ray scattering (SAXS) studies (Figures 2b,d) confirm this exchange of unimers to form blended micelles. From the Porod representation (Figure 2b), the shift in the first oscillation is clearly visible, highlighting the reorganization to blended micelles over time. Furthermore, when the first minima in the SAXS profiles (Figure 2d) are

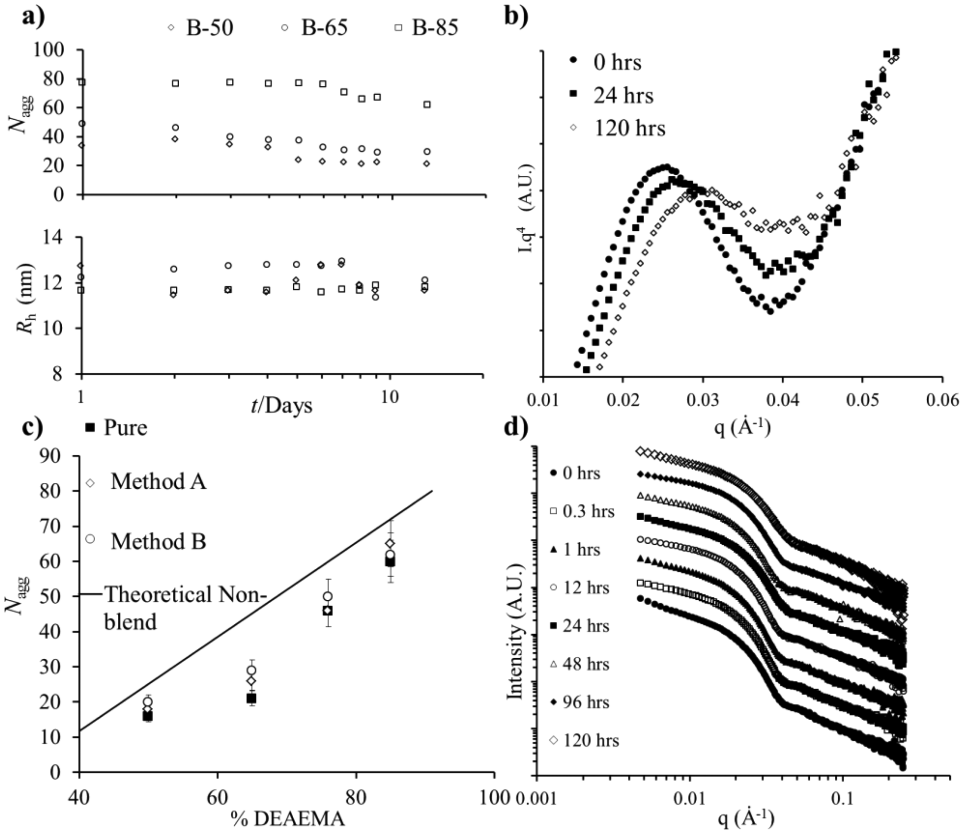

Figure 2. (a) Evolution of aggregation number (N_{agg}) and hydrodynamic radius R_h with time upon blending stock solutions using method B. (b) Porod representation of the SAXS data for **B-76** with time at 2.5 g/L. (c) Relationship of the aggregation number (N_{agg}) at steady state for both blending methods A and B and theoretical aggregation number for a nonblended mixture (straight line) from eq 1 with % DEAEMA in the core domain. N_{agg} of the pure micelles of the same composition as the blends are also given. Error bars are calculated from 10% of the N_{agg} values. (d) SAXS profiles of **B-76** at 2.5 g/L over time; 0 hours indicates the start of the blending for method B. Plots have been shifted vertically for clarity; see Supporting Information for SAXS fits.

DOI: 10.1021/acs.macromol.5b01426
Macromolecules 2015, 48, 6516−6522

compared, we observe a shift to larger q values (from 0.042 to 0.046 Å^{-1}). Both the shifts in Figures 2b,d are representative of a reduction in the core size of the micelles. This reduction in core size is attributed to a decrease in aggregation number as the formation of blended micelles occurs, which is consistent with the light scattering results (Figure 2a).[45]

Structural Comparison of Blended Micelles and Pure Micelles. The blended micelles formed by mixing different ratios of **P-32** and **P-91** (using method A, unimer blending) were compared to those obtained with a pure diblock copolymer matching the average chemical composition of the blend. For these samples, laser light scattering (LLS) (Figures 2c and 3a), SAXS (Figure 3b), and cryogenic transmission

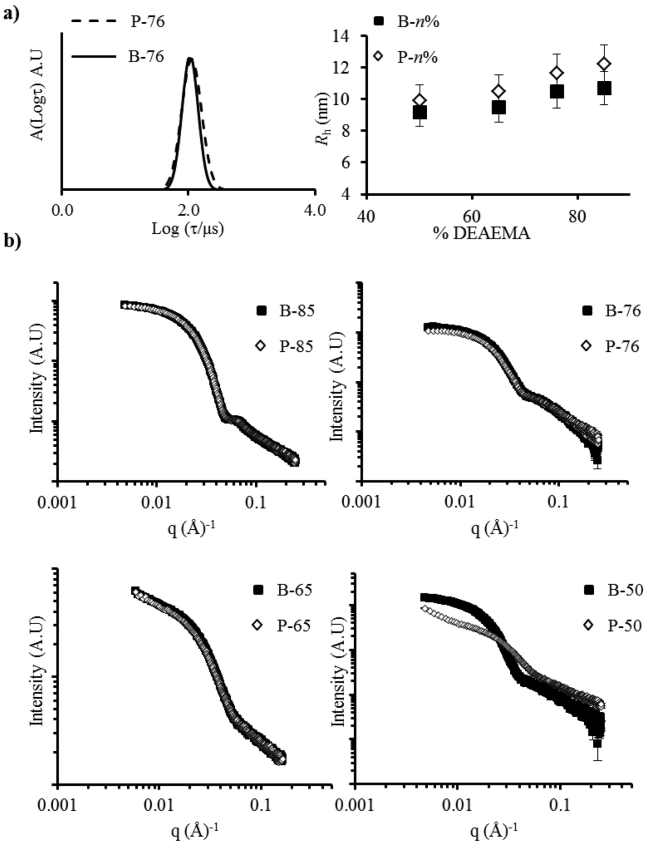

Figure 3. (a) Left pane: relaxation time distribution from DLS of **P-76** and **B-76** at α = 0 in 0.1 M NaCl, at 2.5 g/L obtained by dynamic light scattering; right pane: dependence of hydrodynamic radius (R_h) with % DEAEMA in the core domain. Error bars are calculated from 10% of the R_h values. (b) SAXS profiles of blended and pure samples in NaCl 0.1 M at 2.5 g/L. Note that for the 85%, 76%, and 65% samples the profiles superimpose for the blended and pure solutions. See Table 2 and Table S4 for SAXS fits. All samples were prepared using assembly method A.

electron microscopy (cryo-TEM) (Figure 4) were used to analyze the size (R_h and R_c) of the blended and pure micelles. Remarkably for both the blended and pure micelles above 50% DEAEMA the core sizes are structurally indistinguishable to one another when any of the analysis methods are used (Figure 4 and see Supporting Information for micelle dimensions from SAXS data fits and additional cryo-TEM analysis). However, it should be noted that for 50% DEAEMA (Figure 3b, bottom right pane), a difference between the blended and pure samples is observed. At this composition the pure micelles are only

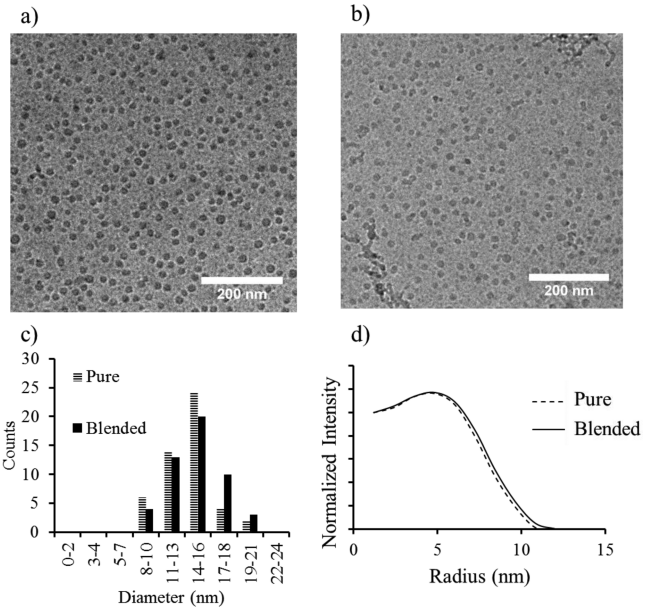

Figure 4. Cryo-TEM analysis of both **P-85** and **B-85** prepared by method A: (a) image of **P-85**; (b) image of **B-85**. (c) Histograms of the core diameter for both **P-85** and **B-85** samples. (d) Radial plot profiles from cryo-TEM for both **P-85** and **B-85** samples (averaged over 50 particles).

weakly associated and exhibit very little contrast between the core and corona. This correlates with critical aggregation concentration studies, CAC (see Supporting Information), where the association of **P-91** was proposed to drive the association of the blended micelles. Furthermore, the blended samples contain a highly aggregating species, and it is hypothesized that this species gives an increased core−corona contrast for the blend assembly. Nevertheless, as both blended and pure systems observed are identical, it is believed that the systems reach equilibrium, where a system at dynamic equilibrium allows for successful blending.[24,46]

Both SAXS and cryo-TEM have the benefit of being able to directly probe the core size of the micellar aggregates in addition to LLS, which allows a theoretical core size to be calculated using eq S6. This allows a comparison of three techniques (LLS, cryo-TEM, and SAXS) to fully analyze the blended and pure micelles (Table 2). A general trend observed is that a decrease in DEAEMA content (from 85% to 50%) gave smaller core sizes. However, the core sizes from cryo-TEM

Table 2. Additional Micelle Scattering Characterization Data for All Blended and Pure Samples at α = 0 in 0.1 M NaCl Solution

	$R_{c,LLS}$ (nm)[a]	$R_{c,cryo\text{-}TEM}$ (nm)	$R_{c,SAXS}$ (nm)	core density based on cryo-TEM[b] (g/L)
P-85	5.1	7.8	8.6	0.17
P-76	4.6	7.8	8.7	0.12
P-65	3.9	6.5	7.6	0.09
P-50	3.3	7.0	5.0	0.05
B-85	5.3	7.3	8.6	0.20
B-76	4.8	7.7	8.8	0.14
B-65	3.9	6.8	7.5	0.09
B-50	3.5	7.4	9.9	0.06

[a]Calculated from eqs S6 and S9 assuming a core density of 1 g/L. [b]Calculated from eq S6 using R_c from cryo-TEM and N_{agg} from SLS.

DOI: 10.1021/acs.macromol.5b01426
Macromolecules 2015, 48, 6516−6522

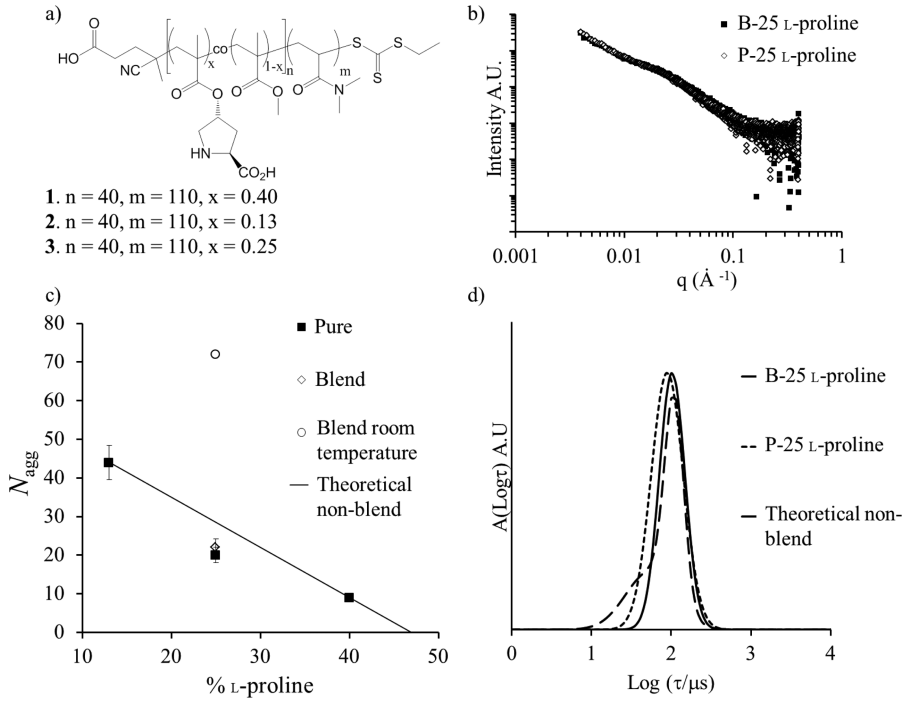

Figure 5. Data for the blended L-proline micelles prepared using unimer blending, method A. (a) Structure of the L-proline diblock copolymers. (b) SAXS analysis of pure and blended L-proline diblock copolymers, at 2.5 g/L note that the profiles superimpose for the blended and pure solutions (see Supporting Information for SAXS fits). (c) Relationship of the experimental aggregation number (N_{agg}) of the blends and of the pure micelles with the same composition with changing % L-proline in the core domain. N_{agg} of the pure micelles of the same composition as the blends are also given. Error bars are calculated from 10% of the N_{agg} values. (d) Relaxation distribution of the pure micelles and blended micelles (at 2.5 g/L) and a theoretical distribution for a nonblended mixture.

and SAXS give slightly larger sizes than calculated from the N_{agg} determined by LLS, which can be attributed to the small contrast difference between the core and corona; therefore, the corona is partially seen.

The core size determined from LLS is calculated assuming that the density of the core is equal to that of the bulk density of the two monomers and is assumed to be constant. However, by using a combination of LLS and cryo-TEM, the core density can be explored further; specifically, a decrease in core density is attributed to an increase in the hydration of the core. This core analysis was explored using a combination of *Z*-average core sizes from cryo-TEM and N_{agg} values from LLS to predict the core density using eq S6; however, the calculated core densities, approximately <0.2 g/mL (Table 2), are too low to provide significant contrast for cryo-TEM, which leads us to believe that the corona must be visible. Moreover, the difference in the scattering length densities between the two monomers for SAXS analysis is extremely small (4.8×10^{-8} Å^{-2}), which results in a portion of the coronal chains being included in the core size when analyzed by SAXS.

Application to Catalytically Active Micelles. This blending method provides a simple and effective route to achieve defined nanoscale assemblies without laborious synthetic approaches. These results demonstrate that the blending strategy can be used to screen both the morphology and function of pure diblock copolymer micelles which can then be adapted for a target application. To highlight the utility of this new approach, we investigated the blending of three diblock copolymers (Figure 5a), with varying incorporations of L-proline in the core domain, to form catalytically active nanostructures.

This strategy allows us to compare the catalytic activity of the pure and blended micelle assemblies and confirm that the proposed strategy is not only relevant from a fundamental point of view but can be used to prepare functional assemblies with targeted properties. As these L-proline block copolymers chemically differ from the pH-responsive methacrylate polymers shown previously, the assembly procedure for these particles was slightly modified (see Supporting Information for details).

Briefly, the powders were mixed and dispersed in water. However, due to the high T_g of methyl methacrylate in the core block, dynamic equilibrium was not reached at room temperature. The solutions were therefore heated to 75 °C for 4 h. The increase in temperature allows for the core block to become more mobile and reduces the energy barrier for molecular exchange thus allowing equilibrium to be reached,[34] resulting in a reorganization of the system as revealed by the difference between the heated and non-heated solutions in Figure 5c.

This reorganization was the first suggestion that blending did occur, provided that the mixing was done at sufficiently high temperature. This was further confirmed using eq S10 which allows for a theoretical relaxation times distribution to be calculated for a nonblended mixture of micelles (see Supporting Information for details). As shown in Figure 5d, the theoretical relaxation distribution does not match the experimentally observed value, indicating that blended micelles are formed rather than a simple mixture of two micelles of different compositions.

Moreover, for these three polymers it was observed that the blended micelles which are formed are identical to the pure copolymer assemblies (Figures 5b,c).

DOI: 10.1021/acs.macromol.5b01426
Macromolecules 2015, 48, 6516−6522

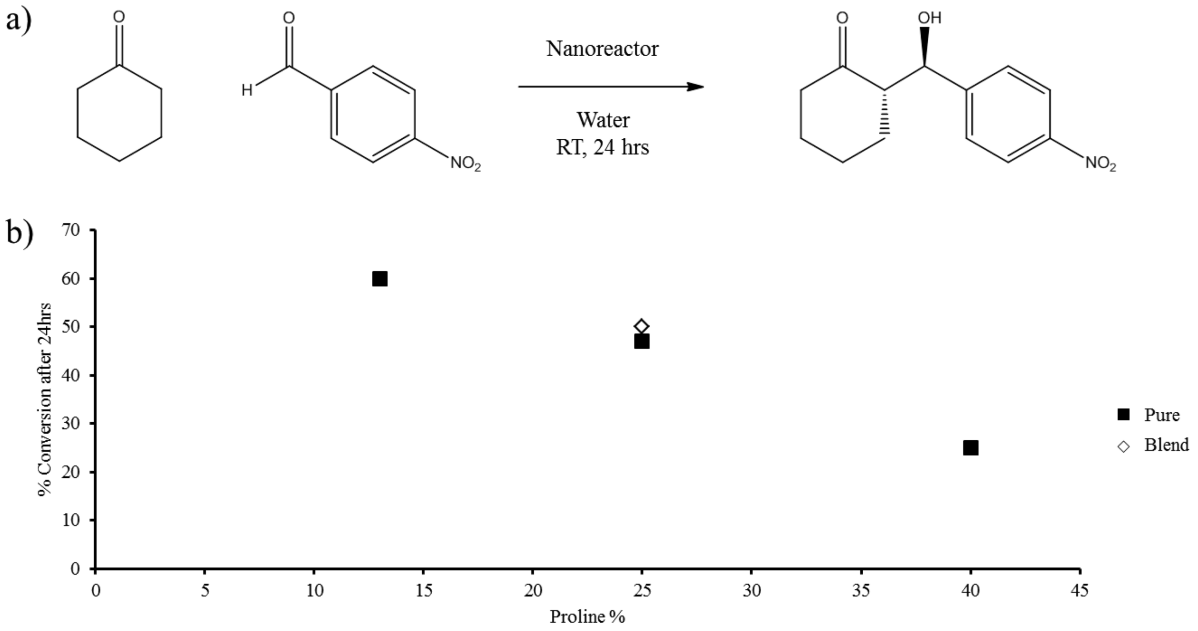

Figure 6. (a) Aldol reaction of 4-nitrobenzaldehyde and cyclohexanone catalyzed by L-proline micelles. (b) Aldol catalysis data for 1 mol% catalyst loading for the pure and blended micelles as determined by ^{1}H NMR spectroscopy.

To understand and evaluate the catalytic performance of these blended micelles compared to the pure micelles, an aldol reaction was undertaken (Figure 6a). An increase in the L-proline content in the core gives a decrease in the conversion after 24 h as previously reported (Figure 6b).[47] The kinetics of the aldol catalysis using the blended (47% conversion for B-25) and pure micelles (50% conversion for P-25) were very similar (Figure 6b).

Given that the concentration of catalyst was constant in these reactions and previous work suggests that the structure of these L-proline micelles dictates the catalytic activity,[48] we can infer that the catalytic environment created in both assemblies are identical. This emphasizes that the copolymer blending method, in which two copolymers of differing compositions are blended, produces micelles which have not only the same structure but the same function as the assemblies prepared from the assembly of a precision copolymer of the same composition.

CONCLUSIONS

A simple copolymer blending method has been utilized to produce a range of polymeric micelles in aqueous solution. In this approach two copolymers with high and low incorporations of hydrophobic monomer are blended to afford a variety of polymeric micelles with varying intermediate hydrophobic compositions. By a combination of cryo-TEM, laser light, and small-angle X-ray scattering methods, these blended micelles were found to be structurally identical to pure micelles with the same composition formed from the direct assembly of a single compositionally pure polymer diblock. This work represents an advantage over traditional approaches for the preparation of spherical nanostructures with specific structural characteristics as it requires minimal synthesis and allows access to the full range of intermediate copolymer compositions through a simple blending approach rather than exhaustive synthesis. We propose this new methodology as a simple, scalable, and effective route to obtain functional block copolymer micelles of diverse compositions and properties as desired for applications such as drug delivery vehicles, stabilizers, or catalytic reactors.

ASSOCIATED CONTENT

Supporting Information

The Supporting Information is available free of charge on the ACS Publications website at DOI: 10.1021/acs.macromol.5b01426.

Additional characterization data, SLS and DLS data, SAXS data, cryo-TEM images, and CAC fluorescent experiments for polymers **P-32**−**P-91**, **B-50**−**B-85**, and L-proline polymers (PDF)

AUTHOR INFORMATION

Corresponding Authors

*E-mail: R.K.O-Reilly@warwick.ac.uk (R.K.O.).
*E-mail: olivier.colombani@univ-lemans.fr (O.C.).
*E-mail: christophe.chassenieux@univ-lemans.fr (C.C.).

Notes

The authors declare no competing financial interest.

ACKNOWLEDGMENTS

The ESF P2M, EPSRC, and AFOSR-DOD are thanked for financial support. We acknowledge cryo-TEM, paid for by the Air Force Office of Scientific Research (PECASE-FA9550-11-1-01-5). A.P.B. and R.K.O. thank Diamond Light Source for access to beamline B21 (proposal SM11120) and Dr. Katsuaki Inoue and Dr. James Doutch for their assistance.

REFERENCES

(1) Hamley, I. W. *The Physics of Block Copolymers*; Oxford University Press: Oxford, 1998.
(2) Hamley, I. W. *Block Copolymers in Solution: Fundamentals and Applications*; Wiley: New York, 2005.
(3) Hayward, R. C.; Pochan, D. J. *Macromolecules* **2010**, *43*, 3577.
(4) Chien, M.-P.; Carlini, A. S.; Hu, D.; Barback, C. V.; Rush, A. M.; Hall, D. J.; Orr, G.; Gianneschi, N. C. *J. Am. Chem. Soc.* **2013**, *135*, 18710.

DOI: 10.1021/acs.macromol.5b01426
Macromolecules 2015, 48, 6516−6522

(5) Bai, Z.; Lodge, T. P. *J. Am. Chem. Soc.* **2010**, *132*, 16265.
(6) Lodge, T. P.; Rasdal, A.; Li, Z.; Hillmyer, M. A. *J. Am. Chem. Soc.* **2005**, *127*, 17608.
(7) Rees, P.; Wills, J. W.; Brown, M. R.; Tonkin, J.; Holton, M. D.; Hondow, N.; Brown, A. P.; Brydson, R.; Millar, V.; Carpenter, A. E.; Summers, H. D. *Nat. Methods* **2014**, *11*, 1177.
(8) Hudson, Z. M.; Lunn, D. J.; Winnik, M. A.; Manners, I. *Nat. Commun.* **2014**, *5*, 3372.
(9) Wever, D. A. Z.; Picchioni, F.; Broekhuis, A. A. *Prog. Polym. Sci.* **2011**, *36*, 1558.
(10) Lu, A.; O'Reilly, R. K. *Curr. Opin. Biotechnol.* **2013**, *24*, 639.
(11) Kelley, E. G.; Albert, J. N. L.; Sullivan, M. O.; Epps, T. H., III *Chem. Soc. Rev.* **2013**, *42*, 7057.
(12) Cotanda, P.; Wright, D. B.; Tyler, M.; O'Reilly, R. K. *J. Polym. Sci., Part A: Polym. Chem.* **2013**, *51*, 3333.
(13) Renou, F.; Nicolai, T.; Nicol, E.; Benyahia, L. *Langmuir* **2009**, *25*, 515.
(14) Palyulin, V. V.; Potemkin, I. I. *Macromolecules* **2008**, *41*, 4459.
(15) Sens, P.; Marques, C. M.; Joanny, J. F. *Macromolecules* **1996**, *29*, 4880.
(16) Tian, M. M.; Qin, A. W.; Ramireddy, C.; Webber, S. E.; Munk, P.; Tuzar, Z.; Prochazka, K. *Langmuir* **1993**, *9*, 1741.
(17) Cantu, L.; Corti, M.; Salina, P. *J. Phys. Chem.* **1991**, *95*, 5981.
(18) Calderara, F.; Riess, G. *Macromol. Chem. Phys.* **1996**, *197*, 2115.
(19) Borovinskii, A. L.; Khokhlov, A. R. *Macromolecules* **1998**, *31*, 7636.
(20) Yoo, S. I.; Sohn, B.-H.; Zin, W.-C.; Jung, J. C.; Park, C. *Macromolecules* **2007**, *40*, 8323.
(21) Hillmyer, M. A. *J. Polym. Sci., Part B: Polym. Phys.* **2007**, *45*, 3249.
(22) Yan, N.; Yang, X.; Zhu, Y.; Xu, J.; Sheng, Y. *Macromol. Chem. Phys.* **2012**, *213*, 2261.
(23) Schuetz, P.; Greenall, M. J.; Bent, J.; Furzeland, S.; Atkins, D.; Butler, M. F.; McLeish, T. C. B.; Buzza, D. M. A. *Soft Matter* **2011**, *7*, 749.
(24) Jain, S.; Bates, F. S. *Macromolecules* **2004**, *37*, 1511.
(25) Tsitsilianis, C.; Gotzamanis, G.; Iatridi, Z. *Eur. Polym. J.* **2011**, *47*, 497.
(26) Shedge, A.; Colombani, O.; Nicolai, T.; Chassenieux, C. *Macromolecules* **2014**, *47*, 2439.
(27) Charbonneau, C. l.; Chassenieux, C.; Colombani, O.; Nicolai, T. *Macromolecules* **2011**, *44*, 4487.
(28) Lejeune, E.; Drechsler, M.; Jestin, J.; Muller, A. H. E.; Chassenieux, C.; Colombani, O. *Macromolecules* **2010**, *43*, 2667.
(29) Bendejacq, D. D.; Ponsinet, V. *J. Phys. Chem. B* **2008**, *112*, 7996.
(30) Bendejacq, D. D.; Ponsinet, V.; Joanicot, M. *Langmuir* **2005**, *21*, 1712.
(31) Borisova, O.; Billon, L.; Zaremski, M.; Grassl, B.; Bakaeva, Z.; Lapp, A.; Stepanek, P.; Borisov, O. *Soft Matter* **2011**, *7*, 10824.
(32) Ribaut, T.; Oberdisse, J.; Annighofer, B.; Stoychev, I.; Fournel, B.; Sarrade, S.; Lacroix-Desmazes, P. *Soft Matter* **2009**, *5*, 4962.
(33) Wright, D. B.; Patterson, J. P.; Pitto-Barry, A.; Cotanda, P.; Chassenieux, C.; Colombani, O.; O'Reilly, R. K. *Polym. Chem.* **2015**, *6*, 2761.
(34) Nicolai, T.; Colombani, O.; Chassenieux, C. *Soft Matter* **2010**, *6*, 3111.
(35) Lund, R.; Willner, L.; Richter, D.; Dormidontova, E. E. *Macromolecules* **2006**, *39*, 4566.
(36) Stejskal, J.; Hlavatá, D.; Sikora, A.; Konňák, Č.; Pleštil, J.; Kratochvíl, P. *Polymer* **1992**, *33*, 3675.
(37) Choi, S.-H.; Lodge, T. P.; Bates, F. S. *Phys. Rev. Lett.* **2010**, *104*, 047802.
(38) Won, Y. Y.; Davis, H. T.; Bates, F. S. *Macromolecules* **2003**, *36*, 953.
(39) Mai, Y.; Eisenberg, A. *Chem. Soc. Rev.* **2012**, *41*, 5969.
(40) Meli, L.; Santiago, J. M.; Lodge, T. P. *Macromolecules* **2010**, *43*, 2018.
(41) Nose, T.; Iyama, K. *Comput. Theor. Polym. Sci.* **2000**, *10*, 249.
(42) Halperin, A.; Alexander, S. *Macromolecules* **1989**, *22*, 2403.
(43) Nyrkova, I. A.; Semenov, A. N. *Macromol. Theory Simul.* **2005**, *14*, 569.
(44) Daoud, M.; Cotton, J. P. *J. Phys. (Paris)* **1982**, *43*, 531.
(45) Patterson, J. P.; Robin, M. P.; Chassenieux, C.; Colombani, O.; O'Reilly, R. K. *Chem. Soc. Rev.* **2014**, *43*, 2412.
(46) Jain, S.; Bates, F. S. *Science* **2003**, *300*, 460.
(47) Lu, A.; Moatsou, D.; Longbottom, D. A.; O'Reilly, R. K. *Chem. Sci.* **2013**, *4*, 965.
(48) Lu, A.; Cotanda, P.; Patterson, J. P.; Longbottom, D. A.; O'Reilly, R. K. *Chem. Commun.* **2012**, *48*, 9699.

DOI: 10.1021/acs.macromol.5b01426
Macromolecules 2015, 48, 6516−6522

Supporting Information

for

The copolymer blending method: A new approach for targeted assembly of micellar nanoparticles

Daniel B. Wright,† Joseph P. Patterson,§ Anaïs Pitto-Barry,† Annhelen Lu,† Nigel Kirby, ‖ Nathan C. Gianneschi,§ Christophe Chassenieux, ‡ Olivier Colombani,* ‡ and Rachel K. O'Reilly*†*

† University of Warwick, Department of Chemistry, Gibbet Hill Road, Coventry CV4 7AL, UK.

‡ LUNAM Université, Université du Maine, IMMM UMR CNRS 6283, Departement PCI, Avenue Olivier Messiaen, 72085 Le Mans, Cedex 09, France.

§ Department of Chemistry & Biochemistry, University of California, 9500 Gilman Drive, La Jolla, CA, 92093, USA.

‖ Australian Synchrotron, 800 Blackburn Road, Clayton, Victoria 3168, Australia

Contents

Methods and Materials

Materials

Monomers were filtered through a plug of silica prior to use and stored at 4 °C. Proline methacrylate was synthesized as previously reported.[1] AIBN (2,2'-azo-bis(isobutyronitrile)) was recrystallized from methanol and stored in the dark at 4 °C. All other materials were used as received from Aldrich, Fluka, and Acros. HCl (1M) and NaOH (1M) were calibrated and standardized using tris(hydroxymethyl)-aminomethane and potassium hydrogen phthalate respectively.

Characterization methods

^{1}H Nuclear magnetic resonance

^{1}H Nuclear magnetic resonance (NMR) spectra were recorded on a Bruker DPX-400 spectrometer in $CDCl_3$. Chemical shifts are given in ppm downfield from TMS.

Size exclusion chromatography

Size exclusion chromatography (SEC) measurements were performed at 40 °C with HPLC grade dimethylformamide (DMF) with 1.06 g/L of LiCl as an eluent and at a flow rate of 1 mL/min. The molecular weights of the synthesized polymers were calculated relative to poly(methyl methacrylate) (PMMA) standards from refractive index traces.

Refractive index increment

The specific refractive index increment (dn/dC) of the polymers in water was measured on a refractometer (Bischoff RI detector) operating at a wavelength of 632 nm. All polymer dn/dC were between 0.121 and 0.129 g/mL at $\alpha = 0$.

Laser light scattering (LLS)

Measurements were performed at angles of observation ranging from 20° up to 130° with an ALV CGS3 setup operating at λ_0 = 632 nm and at 20 °C ± 1 °C. Data were collected in duplicate with 240 s run times. Calibration was achieved with filtered toluene and the background was measured with filtered solvent (NaCl 0.1 M solution).

Dynamic light scattering (DLS)

The normalized intensity autocorrelation functions $g_2(t)$ obtained from dynamic light scattering were related to $g_1(t)$ (the normalized electric field autocorrelation functions) *via* the so-called Siegert relation. Then $g_1(t)$ were analyzed in terms of a continuous distribution of relaxation times (eqn. S1) using the REPES routine[2] without assuming a specific mathematical shape for the distribution of the relaxation times (A(τ)). When comparing micelle distributions directly to one another the Gaus-Gex routine was used.[3]

$$g_1(t) = \int_0^\infty A(\tau) \exp\left(-t/\tau\right) d\tau \qquad \text{(S1)}$$

The apparent diffusion coefficient D was calculated from eqn. S2 given that the z-average relaxation rates τ of the scatterers were q^2-dependent, where q is the scattering vector given by $q = (4\pi n/\lambda_0)\sin(\theta/2)$ with θ the angle of observation and n = 1.333 the refractive index of the solvent (water).

$$D = 1/\tau q^2 \qquad \text{(S2)}$$

The concentration dependence of D is given by $D = D_0(1+k_DC)$ where k_D is the dynamic second virial coefficient and D_0 the diffusion coefficient used for computing the hydrodynamic radius (R_h) of the scatterers according to the Stokes-Einstein equation (eqn. S3).

$$D_0 = \frac{kT}{6\pi\eta R_h} \qquad \text{(S3)}$$

With η the solvent viscosity, k Boltzmann's constant and T the absolute temperature. Values of R_h given in the following are then obtained after extrapolation to zero concentration.

Static light scattering (SLS)

The Rayleigh ratio of the solutions have been measured using toluene as a reference according to: $R_\theta = (I_{solution}(\theta)-I_{solvent}(\theta))/I_{toluene}(\theta).R_{tol}$ where I_i represents the intensity scattered by species i and R_{tol} is the Rayleigh ratio of the reference. We use typically $R_{tol} = 1.35 \times 10^{-5}$ cm^{-1} the Rayleigh ratio of toluene for a wavelength λ = 632.8 nm. In dilute solutions if $R_g.q < 1$ where R_g is the radius of gyration, the q and concentration dependence of R_θ is given by: (eqn S4).

$$\frac{KC}{R_\theta} = \left(\frac{1}{M_w} + 2A_{2C}\right)\left(1 + \frac{q^2 {R_g}^2}{3}\right) \qquad \text{(S4)}$$

Where A_2 is the second virial coefficient and M_w the weight average molecular weight. K is an optical constant given by (eqn. S5):

$$K = \frac{4\pi^2 no^2}{\lambda^4 N_a}\left(\frac{dn}{dC}\right)^2 \qquad \text{(S5)}$$

Where $n_o = 1.496$ is the refractive index of the reference liquid (toluene), dn/dC is the specific refractive index increment determined by differential refractometry and N_A is Avogadro's number. Values of M_w are then obtained after extrapolation to zero concentration and angle and used to derive the aggregation number of the micellar aggregates $N_{agg} = M_{w,aggregate}/M_{w,unimers}$. For spherical morphologies, it is possible to deduce the core radius, R_c, from the aggregation number, using equation S6 assuming the core block is dehydrated and its density matches that of the bulk value, ρ, which is assumed to be constant.[4]

$$\frac{4\pi\rho {R_c}^3}{3} = N_{agg}\frac{M_{W\ Hydrophobic\ block}}{N_a} \qquad \text{(S6)}$$

When in some cases two modes of relaxation were observed by DLS measurements, R_θ was described as the sum of a fast and a slow contribution according to (eqn. S7).

$$R_\theta = R_{\theta f} + R_\theta s \qquad \text{(S7)}$$

Where f and s stand respectively for fast and slow and using equation S8 $R_{\theta f}$ could be calculated:

$$R_{\theta f}(q) = \frac{A_f(q)}{\left(A_f(q) + A_s(q)\right)}R_\theta \qquad \text{(S8)}$$

Where A_f and A_s are the relative amplitudes of the fast and slow modes obtained by DLS. The slow mode of relaxation when observed can be attributed to spurious aggregates with a negligible weight

fraction but larger scattering intensity.[5-7] Consequently, only the fast mode was taken into account, assuming that the polymer concentration involved in the fast mode corresponded to the macroscopic polymer concentration.

Using a combination of DLS and SLS, for spherical morphologies it is possible to deduce the coronal stretching, using equation S9, where 0.25 is the bond length in nanometres of a vinyl repeat unit along the polymer chain.

$$Coronal\ stretching = \frac{(R_h - R_{core})}{(0.25 \times Degree\ of\ Polymerisation_{corona})} \quad \text{(S9)}$$

Small angle X-ray scattering (SAXS).

Measurements were performed at the Australian Synchrotron facility at a photon energy of 11 keV. Measurements for the L-proline systems were performed at Diamond Light Source on beamline B21 at a photon energy of 12.4 keV. Samples were collected at a sample to detector distance of 3.932 m to give a q range of 0.004 to 0.4 $Å^{-1}$The samples in solutions of 0.1 M NaCl were collected at a sample to detector distance of 3.252 m to give a q range of 0.004 to 0.2 $Å^{-1}$. The scattering from a blank (aqueous solution of NaCl 0.1 M) was measured in the same location as the sample collection and was subtracted for each measurement. Data were normalized for total transmitted flux using a quantitative beamstop detector and absolute scaled using water as an absolute intensity standard. The two-dimensional isotropic SAXS images were converted into one-dimensional SAXS scattered intensity profiles ($I(q)$ *versus* q) by circular averaging. The functions used for the fitting from NCNR package[8] were "Guinier-Porod"[9,10], "Polycore Form"[10] and "Debye"[11]. Scattering length densities (SLD) were calculated using the "Scattering Length Density Calculator"[12] provided by the NIST Center for Neutron Research. A linear summation of the PolyCoreShell ratio model and the Debye model is used and has the following parameters (K0 to K7 for the PCR model, K8 to K10 for the Debye model):

K0 scale

K1 average core radius (Å)

K2 average shell thickness (Å), not used in this model

K3 overall polydispersity

K4 scattering length density (SLD) core ($Å^{-2}$)

K5 SLD shell ($Å^{-2}$), not used in this model

K6 SLD solvent ($Å^{-2}$)

K7 background (cm^{-1})

K8 scale

K9 R_g (Å), used in this model as a hydrated thickness, and as unimers in solution for the kinetics early data points

K10 background (cm^{-1})

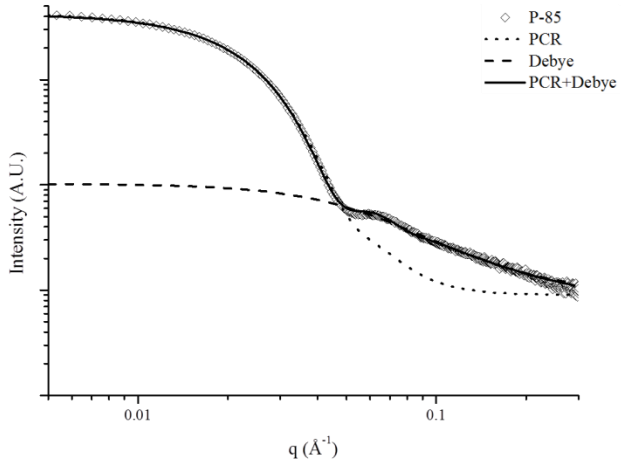

Figure S1. SAXS profile of **P-85** showing the Debye model fit, PolyCoreShell model fit and a linear summation of the PolyCoreShell and Debye model fit.

Cryogenic transmission electron microscopy samples (cryo-TEM).

Cryo-TEM was conducted on a FEI Sphera microscope operated at 200 keV. 3.5 μL of sample was added to freshly glow discharged Quantifoil R2/2 TEM grids. The grids were blotted with filter paper under high humidity to create thin films and rapidly plunged into liquid ethane. The grids were transferred to the microscope under liquid nitrogen and kept at < -175 °C while imaging.

Pyrene fluorescence spectroscopy.

Fluorescence spectra were collected on a PerkinElmer LS 55 Fluorescence Spectrometer. Stock solutions of the polymers were first prepared at 1 g/L using the pure micelle assembly method and method A (unimer mixing) for the blended micelles. These stock solutions were then subsequently diluted to give a range of concentrations from 1×10^{-3} g/L to 1 g/L. Each sample was then prepared by dropping 10 μL of a pyrene solution (6×10^{-5} mol/L in acetone) into an empty vial. These vials were left open overnight to allow the acetone to evaporate. Following this the polymer samples were added to each vial, these solutions were left to equilibrate under stirring for 2 days before analysis. The final pyrene concentration in solution was 6×10^{-7} mol/L. The excitation spectra were recorded with an emission wavelength of 390 nm.

Synthetic methods

General procedure for copolymerization of DMAEMA with DEAEMA to afford MacroCTA.

A solution of 40 equivalents of a combination of the two monomers (DMAEMA = x, DEAEMA = 40-x), 0.2 equivalents of AIBN and 1 equivalent of 2-cyano-2-propyl dithiobenzoate (CPDB) in 1,4-dioxane (1:1 volume compared to monomer) was added to a dry ampoule containing a stirrer bar. The solution was degassed using at least 3 freeze-pump-thaw cycles, back filled with nitrogen, sealed and placed in a pre-heated oil bath at 70 °C. After 7 hours the polymerization was quenched by liquid nitrogen, dioxane removed *in vacuo* and the resultant polymer diluted with H_2O. The solution was transferred to a dialysis membrane tube with the appropriate molecular weight cut-off (MWCO 3.5 kDa) and dialyzed against 18.2 MΩ.cm water (1.5 L) with 3 water changes. Lyophilization resulted in a pink copolymer which is further extended in the next synthesis step. ^{1}H NMR (400 MHz, $CDCl_3$): δ (ppm) 7.85 (d, J = 8.1 Hz, 1H Ar end group), 7.55 (t, J = 7.4 Hz, 2H end group), 7.41 (t, J = 8.1 Hz, 2H, end group), 4.20 (br t, 2H, OCH_2CH_2N), 2.50 (br s, 2H, OCH_2CH_2N), 2.30 (br t, 4H, $OCH_2CH_2N(CH_2)_2(CH_3)_2$), 2.10 (br s, 6H, $OCH_2CH_2N(CH_3)_2$), 1.94 (s, 6H, end group), 1.10 (br t, 6H, $OCH_2CH_2N(CH_2)_2(CH_3)_2$), 1.00-2.00 (br m, backbone) (See Table 1 for molecular weight data).

General procedure for chain extension of the copolymers with DMAEMA.

MacroCTA (1.0 eq), AIBN (0.2 eq) and DMAEMA (40 eq) were dissolved in DMF (1:1 volume compared to the monomer) and were added to a dry ampoule containing a stirrer bar. The solution was degassed using at least 3 freeze-pump-thaw cycles, back filled with nitrogen, sealed and placed in a pre-heated oil bath at 70 °C. After 7 hours the polymerization was quenched by liquid nitrogen, DMF was removed *in vacuo* and the resultant polymer diluted with H_2O and transferred to a dialysis membrane tube with the appropriate molecular weight cut off (MWCO 6 - 8 kDa) and dialyzed against 18.2 MΩ.cm water (1.5 L) with 3 water changes. Lyophilization resulted in a pink polymer.

^{1}H NMR (400 MHz, $CDCl_3$): δ (ppm) 7.85 (d, J = 8.1 Hz, 1H end group), 7.55 (t, J = 7.4 Hz, 2H end group), 7.41 (t, J = 8.1 Hz, 2H, end group), 4.20 (br t, 2H, OCH_2CH_2N), 2.50 (br s, 2H, OCH_2CH_2N), 2.30 (br t, 4H, $OCH_2CH_2N(CH_2)_2(CH_3)_2$), 2.10 (br s, 6H, $OCH_2CH_2N(CH_3)_2$), 1.94 (s, 6H, end group), 1.10 (br t, 6H, $OCH_2CH_2N(CH_2)_2(CH_3)_2$), 1.00-2.00 (br m, backbone) (See Table 1 for molecular weight data).

General procedure for copolymerization of ProMA with MMA.

A solution of 45 equivalents of a combination of the two monomers (L-Proline methacrylate, ProMA= x, MMA = 45 - x), 0.2 equivalents of AIBN and 1 equivalent of 4-cyano-4-[(ethylsulfanylthiocarbonyl) sulfanyl]pentanoic acid in DMSO (1:1 volume compared to monomer) were added to a dry ampoule containing a stirrer bar. The solution was degassed using at least 3 freeze-pump-thaw cycles, back filled with nitrogen, sealed and placed in a pre-heated oil bath at 70 °C. After 5 hours, (approximately 90% conversion) the polymerization was quenched using liquid nitrogen, the DMSO removed *in vacuo* and the resultant polymer diluted with dichloromethane and precipitated into cold MeOH. This resulted in a yellow copolymer which was further chain extended in the next synthesis step.

General procedure for chain extension of the copolymers with DMA.

MacroCTA (1.0 eq), AIBN (0.2 eq) and dimethyl acrylamide, DMA (110 eq) were dissolved in DMSO (1:1 volume compared to the monomer) and were added to a dry ampoule containing a stirrer bar. The solution was degassed using at least 3 freeze-pump-thaw cycles, back filled with nitrogen, sealed and placed in a pre-heated oil bath at 70 °C. After 3 hours (approximately 99% conversion) the polymerization was quenched using liquid nitrogen, the DMSO removed *in vacuo* and the resultant

polymer diluted with dichloromethane and precipitated into cold *n*-hexane resulting in a yellow copolymer.

Table S1. Characteristics of the P(MMA_{1-x}-*co*-$ProMA_x$)$_n$-*b*-$PDMA_m$ diblock copolymers.

Diblock Copolymer	x[a]	n[a]	m[a]	Mol% L-proline in core block[a]	$M_{n,NMR}$[b] (kDa)	d*n*/d*C* [c] (mL/g)
1	0.40	40	110	40	15.9	0.122
2	0.13	40	110	13	15.2	0.125
3	0.25	40	110	25	15.5	0.124

[a] Determined by ^{1}H NMR spectroscopy. [b] Determined by end-group analysis from ^{1}H NMR spectroscopy. [c] Determined by differential refractometery in 18.2 MΩ.cm water.

Preparation of the aqueous solutions of P(DMAEMA-*co*-DEAEMA)-*b*-PDMAEMA diblock copolymers.

Pure micelle samples

Pure micelle assembly was performed by diluting stock polymer solutions that were prepared at 20 g/L by dispersing the polymer in 18.2 MΩ.cm water containing the appropriate amount of HCl to reach α = 1, where α is defined as, $\alpha = [NR_2H^+]/[NR_{2Total}]$. After one night of stirring α was lowered to α = 0 by the addition of the required amount of 1 M NaOH and the solutions were stirred again overnight, after which time the NaCl concentration was adjusted to 0.1 M by the addition of 4 M NaCl. The solutions were further stirred overnight before dilution to 2.5 g/L prior to analysis.

Blended micelle samples.

Two methods for the preparation of the binary solutions were used.

Method A (unimer blending) consisted of mixing dry bulk polymer samples together. These dry powders were then used to produce polymer solutions at 10 g/L which were prepared by dispersing the two polymer powders in 18.2 MΩcm water containing the appropriate amount of HCl to reach $\alpha = 1$ to give a solution of blended unimers in a good solvent. After one night of stirring α was lowered to 0 by the addition of the required amount of 1 M NaOH and the solutions were stirred again overnight, after which time the NaCl concentration was adjusted to 0.1 M by the addition of 4 M NaCl. The solutions were further stirred overnight before being diluted to 2.5 g/L for analysis.

Method B (micelle blending) involved making individual polymer solutions of 32% DEAEMA and 91% DEAEMA copolymers at $\alpha = 0$ using the same protocol as for the pure micelle samples, at a concentration of 2.5 g/L. These solutions were then poured together at desired stoechiometric ratios and stirred to give the targeted % DEAEMA and then stored at room temperature.

Preparation of the L-proline-based polymer aqueous solutions.

Pure L-proline micelle assembly was performed using a direct dissolution method by dispersing the dry polymer powder in 18.2 MΩ.cm water. The solution was then sealed and heated to 75 °C for 4 hours whilst stirring. After this time the solutions were left to cool to room temperature and stirred overnight before analysis. For the blended L-proline micelle samples, the appropriate ratios of the two polymer powders were first weighed together and then the blended powder was dispersed as described above.

Characteristics of the P(DMAEMA-*co*-DEAEMA)-*b*-PDMAEMA diblock copolymers

Table S2. Molar mixing ratios for the blended block copolymers systems.

Blended diblock copolymer	Mole fraction of **P-91**	Mole fraction of **P-32**	Theoretical % of DEAEMA in core block
B-50	0.40	0.60	50
B-65	0.60	0.40	65
B-76	0.75	0.25	76
B-85	0.90	0.10	85

Table S3. SAXS parameters for **P-85**, **B-85**, **P-76**, **B-76** in Figure 3. Values are given as provided by the software.

	P-85	**B-85**	**P-76**	**B-76**
K0	$5.0699\ 10^{-4} \pm 1.43\ 10^{-7}$	$5.1212\ 10^{-4} \pm 1.54\ 10^{-7}$	$5.7959\ 10^{-5} \pm$ 0.000128	6.3606e-005 ± 0.000109
K1	85.512 ± 0.016	86.295 ± 0.019	87.109 ± 0.0661	88.471 ± 0.0659
K2[a]	0 ± 0	0 ± 0	0 ± 0	0 ± 0
K3	$0.1613 \pm 8.96\ 10^{-5}$	0.1620 ± 0.00013	0.1813 ± 0	0.17587 ± 0
K4[c]	$8.643\ 10^{-6} \pm 0$	$8.638\ 10^{-6} \pm 0$	$8.643\ 10^{-6} \pm 0$	$8.643\ 10^{-6} \pm 0$
K5[a]	$8.638\ 10^{-5} \pm 0$	$8.638\ 10^{-5} \pm 0$	$8.638\ 10^{-5} \pm 0$	$8.638\ 10^{-5} \pm 0$
K6	$1.0197\ 10^{-5} \pm 0$	$1.0197\ 10^{-5} \pm 0$	$1.0197\ 10^{-5} \pm 0$	$1.0197\ 10^{-5} \pm 0$
K7[b]	0 ± 0	0 ± 0	0 ± 0	0 ± 0
K8	$0.0033612 \pm 1.04\ 10^{-5}$	$0.0033887 \pm 1.07\ 10^{-5}$	$0.0026887 \pm 1.66\ 10^{-5}$	$0.0031012 \pm 4.24\ 10^{-5}$
K9	13.365 ± 0.0792	13.348 ± 0.0806	18.733 ± 0.0984	18.813 ± 0.207
K10	0.0006 ± 0	0.0006 ± 0	0.0001 ± 0	0.0001 ± 0

[a] K2 and K5 are not used in this model as we only use the core part of the PCR model thus the value of thickness is set equal to zero and the value of the SLS of the shell is set to a random value. [b] One of the two background parameters has to be set equal to zero according to the NIST package for summation. [c] The SLD value for the core is not set free and is calculated knowing the density of the monomers in the core block, the chemical formula and the energy of the SAXS beam with a free program on the NIST website.[13]

Table S4. SAXS parameters for **P-65**, **B-65**, **P-50**, **B-50** in Figure 3. Values are given as provided by the software.

	P-65	**B-65**	**P-50**	**B-50**
K0	0.00011143 ± 6.48 10^{-7}	0.00010759 ± 5.6 10^{-7}	8.9243 10^{-5} ± 0.000186	9.2814 10^{-5} ± 0.000109
K1	75.161 ± 0.493	74.869 ± 0.409	49.917 ± 0.618	98.953 ± 0.12
K2[a]	0 ± 0	0 ± 0	0 ± 0	0 ± 0
K3	0.35537 ± 0.00461	0.27096 ± 0.00359	0.36013 ± 0.00589	0.20964 ± 0.00074
K4[c]	8.649 10^{-6} ± 0	8.649 10^{-6} ± 0	8.656 10^{-6} ± 0	8.656 10^{-6} ± 0
K5[a]	8.638 10^{-5} ± 0	8.638 10^{-5} ± 0	8.638 10^{-5} ± 0	8.638 10^{-5} ± 0
K6	1.0197 10^{-5} ± 0	1.0197 10^{-5} ± 0	1.0197 10^{-5} ± 0	1.0197 10^{-5} ± 0
K7[b]	0 ± 0	0 ± 0	0 ± 0	0 ± 0
K8	0.0026236 ± 2.39 10^{-5}	0.0029294 ± 2.89 10^{-5}	0.0022803 ± 3.36 10^{-5}	0.0015219 ± 1.6 10^{-5}
K9	14.399 ± 0.105	16.67 ± 0.124	17.733 ± 0.185	18.057 ± 0.166
K10	0.0009 ± 0	0.001 ± 0	0.0004 ± 0	0.0001 ± 0

[a] K2 and K5 are not used in this model as we only use the core part of the PCR model thus the value of thickness is set equal to zero and the value of the SLS of the shell is set to a random value. [b] One of the two background parameters has to be set equal to zero according to the NIST package for summation. [c] The SLD value for the core is not set free and is calculated knowing the density of the monomers in the core block, the chemical formula and the energy of the SAXS beam with a free program on the NIST website.[13]

Pyrene fluorescence experiments on the P(DMAEMA-*co*-DEAEMA)-*b*-PDMAEMA diblock copolymers.

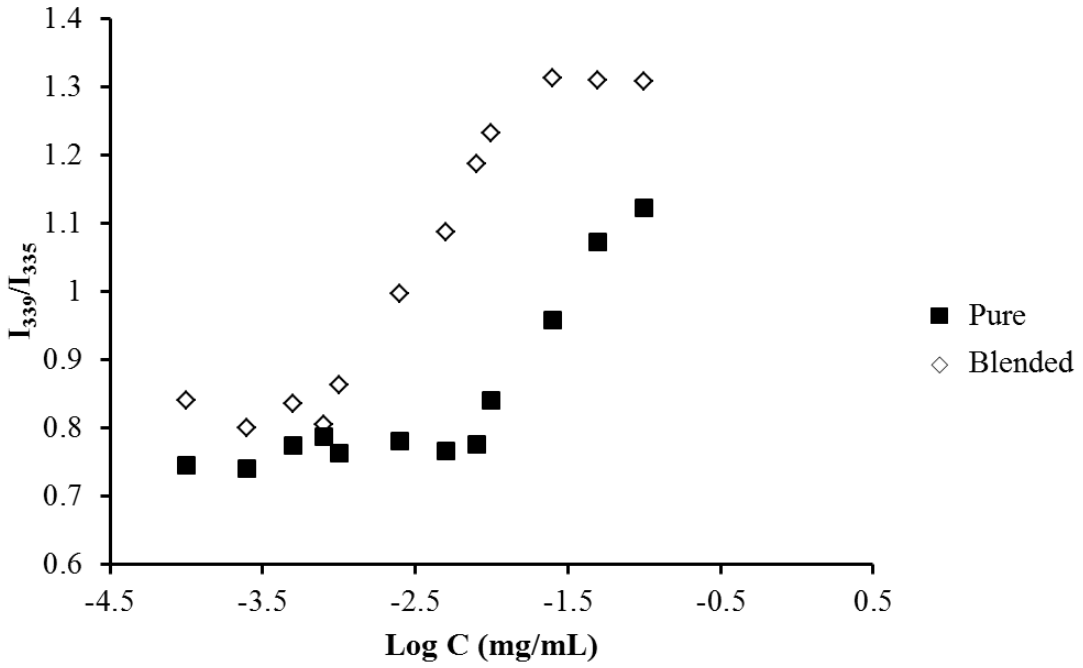

Figure S2. Intensity ratio I_3/I_1 from the steady state fluorescence of pyrene as a function of polymer concentration; data shown is for **P-65** and **B-65,** prepared using Method A.

By using the steady state fluorescence spectroscopy of pyrene we can understand the formation of both the pure and mixed micelles. The principle of the method is based on the fact that the emission of pyrene depends on the polarity of its surrounding medium. Therefore, when pyrene is encapsulated in the micelles, an increase in the ratio of the absorbance at 339 nm compared to 335 nm intensity is observed,[14] and analyzing this ratio with concentration allows for a precise CAC determination. The CAC is taken from the inflection point of the intensity ratios *versus* concentration.

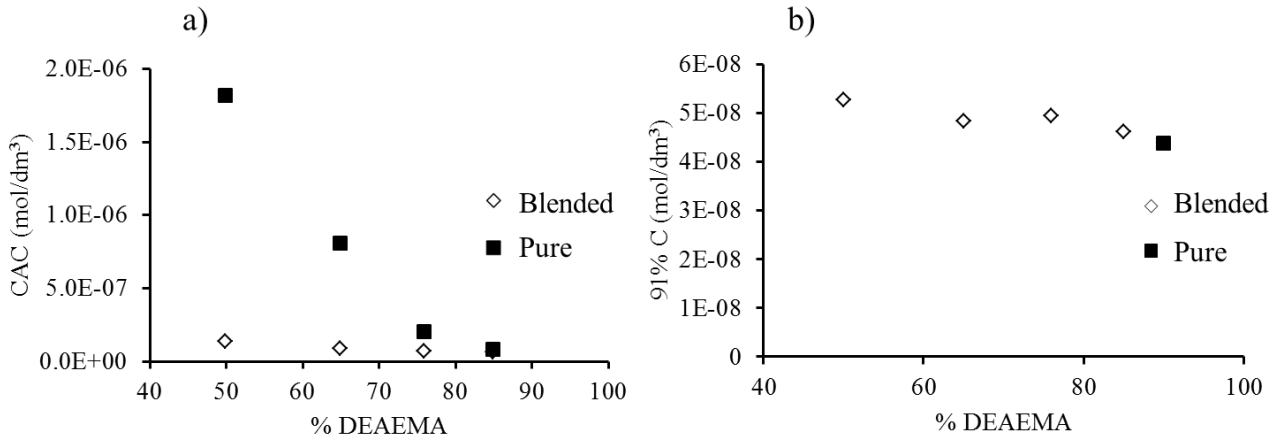

Figure S3. a) Evolution of the CAC as a function of %DEAEMA in the core for pure and blended micelles. b) Concentration of **P-91** in the solution at the CAC for pure and blended micelles.

A clear difference in the steady state fluorescence results of pyrene was observed. For the pure micelles we note that as the DEAEMA content increased the critical aggregation concentration (CAC) decreased. However, the contrary is seen for the blended systems as all DEAEMA core loadings show very similar CAC values, approximately 4.9×10^{-4} mol/dm^3, comparable to that of the pure micelle sytem for **P-91**. Plotting the concentration of **P-91** in the blended system at the CAC for the micelles we observe that the values are extremely similar, Figure S3b. The concentration of P-91 at the CAC value in Figure S3b was calculated by multiplying the CAC values from Figure S3a by the blending ratio of **P-91** in Table S3 for each % DEAEMA incorproation. At this point we are unable to distinguish if these results are representative of a true CAC or the partition equilibrium of pyrene between the micelle cores and the aqueous solvent. We can consider two possible scenarios may be occuring. Firstly, as the DEAEMA content decreases in the pure micelles there is a decrease in the core hydrophobicity. This decrease in core hydrophobicity means that pyrene is less efficiently encapsulated within the cores and the equilibrum is shifted causing more pyrene to reside in the aqueous solution and a higher CAC is observed. However for the blended system a different scenario is present, here it can be deduced that the

P-32 polymer can encapsulate negligible levels of pyrene whereas the P**-91** polymer can encapsulate much larger amounts of pyrene. Therfore only when **P-91** polymers are present can pyrene effectively partition into the core. The second scenerio which could be occuring is that we are observing a true CAC for the micelles. For the pure system a decrease in CAC with increasing DEAEMA content is to be expected due to the increased hydrophobicity of the polymer chains and incompatability with the solvent. Hence, micelles with high DEAEMA content form at lower concentrations.

Cryo-TEM of the P(DMAEMA-*co*-DEAEMA)-*b*-PDMAEMA diblock copolymers.

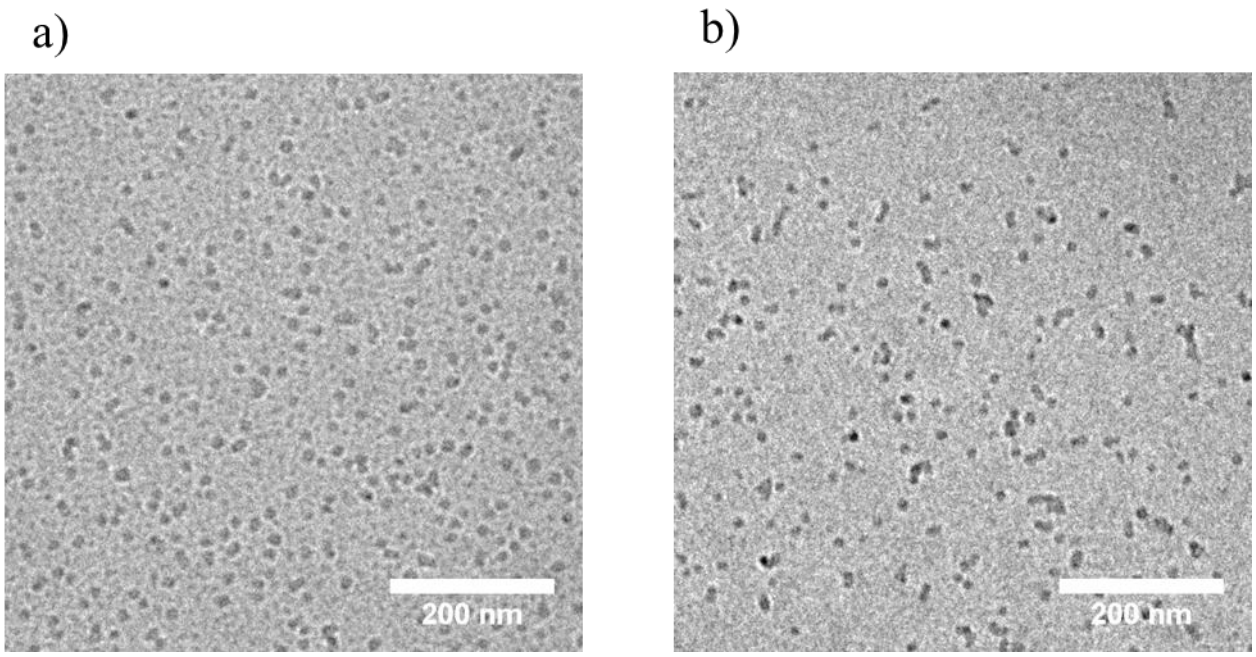

Figure S4. Cryo-TEM images for a) **P-50** and b) **B-50** (Method A) at 2 g/L in 0.1 M NaCl solution.

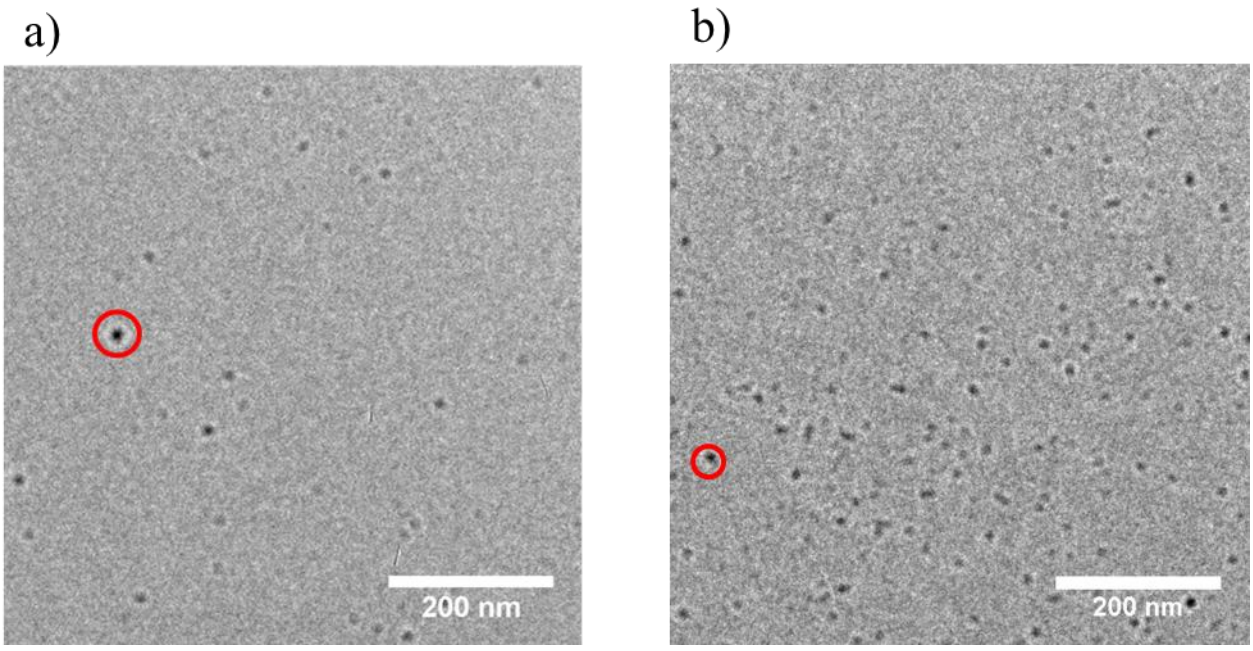

Figure S5. Cryo-TEM images for a) **P-65** and b) **B-65** (Method A) at 2 g/L in 0.1M NaCl solution. The red circles indicate ice crystals.

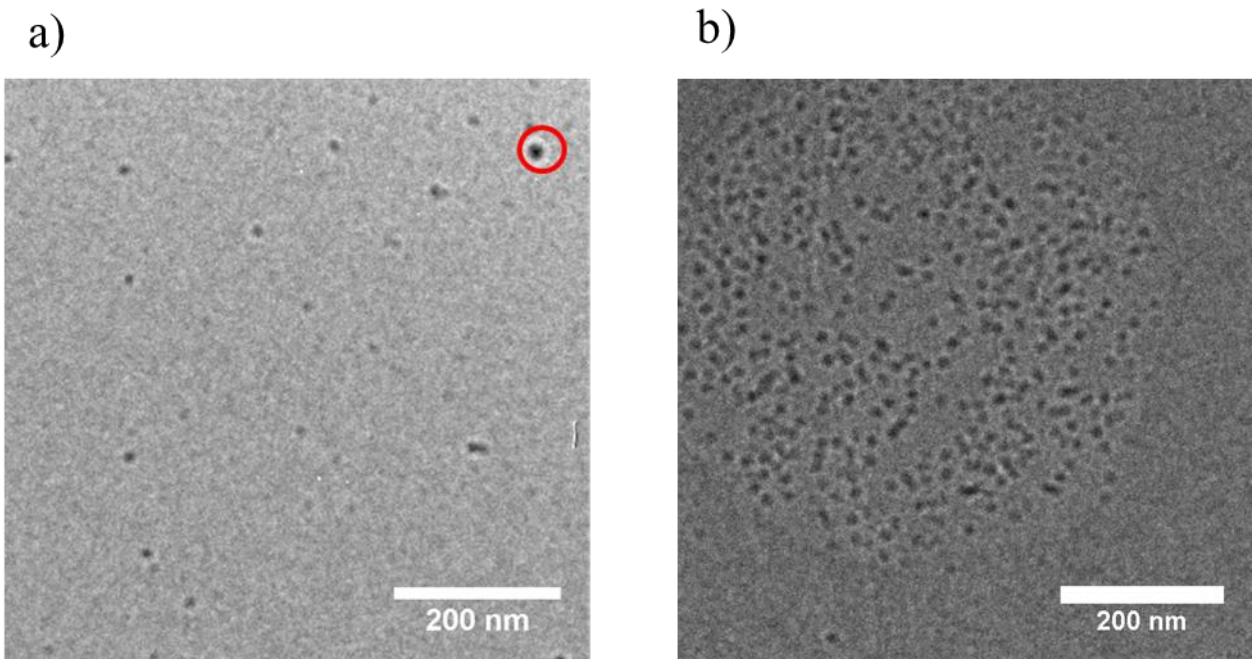

Figure S6. Cryo-TEM images for a) **P-76** and b) **B-76** (Method A) at 2 g/L in 0.1 M NaCl solution. The red circles indicate ice crystals.

Comparison of the cryo-TEM, LLS and SAXS data for the P(DEAEMA-*co*-DMAEMA)-*b*-PDMAEMA diblock copolymers.

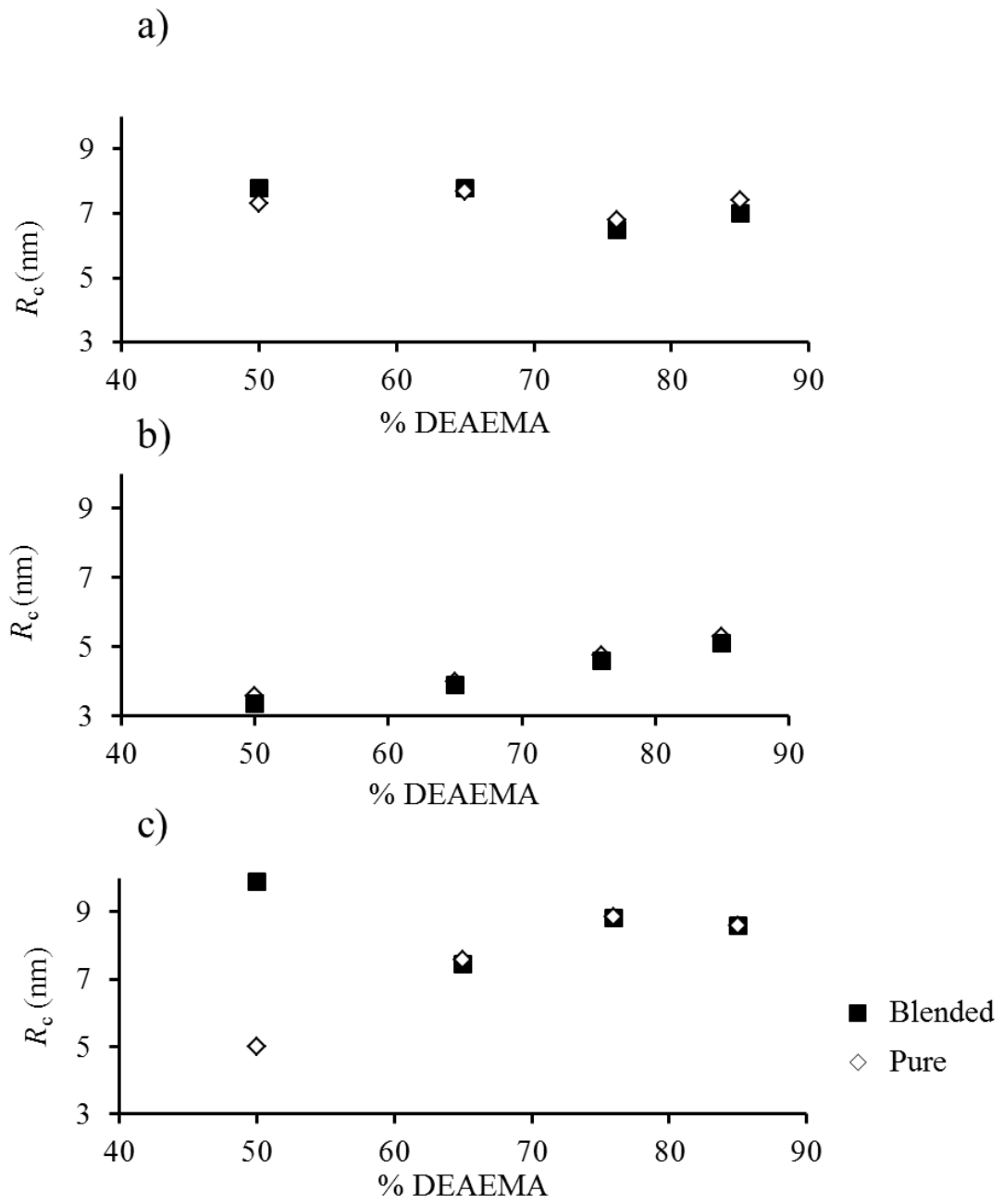

Figure S7. Comparison of core sizes from a) cryo-TEM, b) LLS and c) SAXS for unimer blending (Method A) and pure micellar assembly.

Table S5. Additional micelle scattering characterization data for all blended and pure samples at $\alpha = 0$ in 0.1 M NaCl solution.

	N_{agg}	$R_{h\ LLS}$ (nm)	$R_{c\ LLS}$ (nm)[a]	Coronal Stretching (%)[a]	$R_{c\ cryo\text{-}TEM}$ (nm)	$R_{c\ SAXS}$ (nm)	R_{SAXS} (nm)	Core density based on cryo-TEM (g/L)[b]
P-91	80	10.1	5.6	56	-	-	-	-
P-85	60	10.7	5.1	64	7.8	8.6	10.1	0.17
P-76	46	10.5	4.6	70	7.8	8.7	10.5	0.12
P-65	21	9.5	3.9	64	6.5	7.6	8.9	0.09
P-50	16	9.2	3.3	73	7.0	5.0	8.3	0.05
P-32	1	3.0	[c]	[c]	-	-	-	-
B-85	65	12.2	5.3	87	7.3	8.6	10.1	0.20
B-76	46	11.7	4.8	86	7.7	8.8	10.3	0.14
B-65	26	10.5	3.9	74	6.8	7.5	8.9	0.09
B-50	18	9.9	3.5	87	7.4	9.9	12.6	0.06

[a] Calculated from equations S6 and S9 assuming a core density of 1 g/L. [b] Calculated from equation S6 using R_c from cryo-TEM and N_{agg} from SLS. [c] The model of a "core-corona" is not applicable.

Using the combination of cryo-TEM, SAXS and LLS a spherical morphology can be further confirmed. As observed by cryo-TEM the particles are clearly spherical in nature. However, due to contrast variations the true nature of these spherical particles cannot be further deduced from microscopy. Therefore a simple core-corona model can be used with LLS; as such the dimensions from this model are consistent with a spherical micelle morphology where the coronal chains are moderately stretched (Table S5).

Comparison of the relaxation time distribution for the pure and blended micelles of P(DMAEMA-*co*-DEAEMA)-*b*-PDMAEMA diblock copolymers.

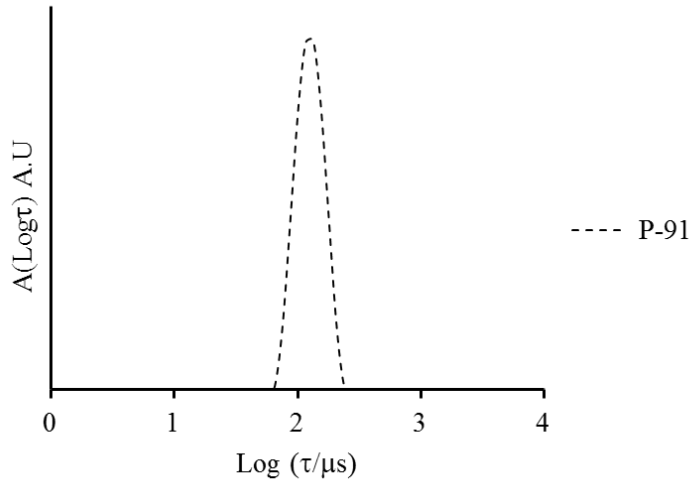

Figure S8. Relaxation time distribution of **P-91** at $\alpha = 0$ in 0.1 M NaCl solution, measured at $\theta = 130°$.

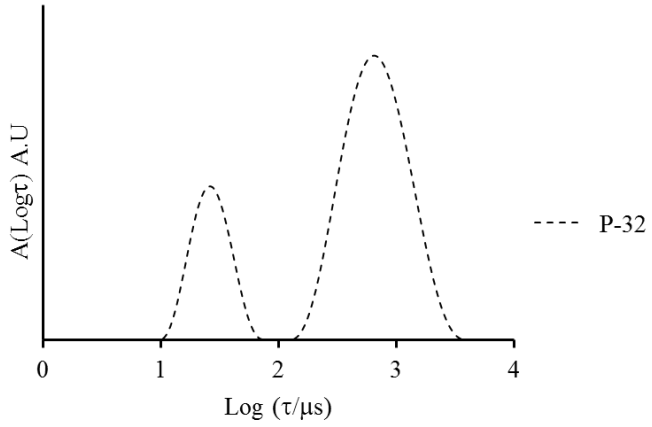

Figure S9. Relaxation time distribution of **P-32** at $\alpha = 0$ in 0.1 M NaCl solution, measured at $\theta = 130°$. Note that although the slow mode scatters the most, it corresponds to a negligible weight fraction of polymer. Indeed, the slow mode corresponds to aggregates about 30 times as large as those corresponding to the fast mode. Considering that the intensity is proportional at least to the size of the aggregates to the power of 2 or 3, the slow mode represents much less than 1% by weight of the total sample and can therefore be neglected.

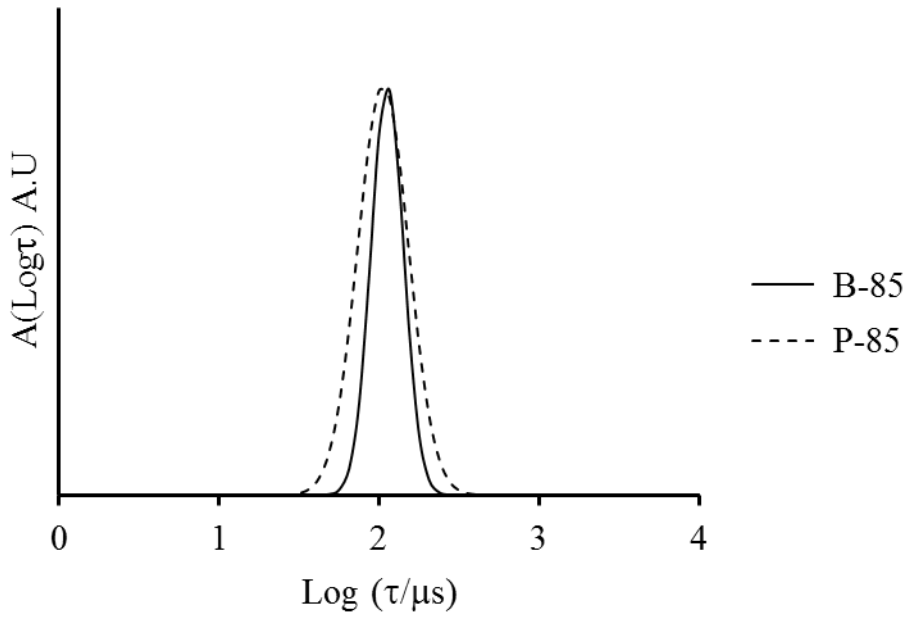

Figure S10. Relaxation time distribution of **P-85** and **B-85** at $\alpha = 0$ in 0.1 M NaCl solution, measured at $\theta = 130°$.

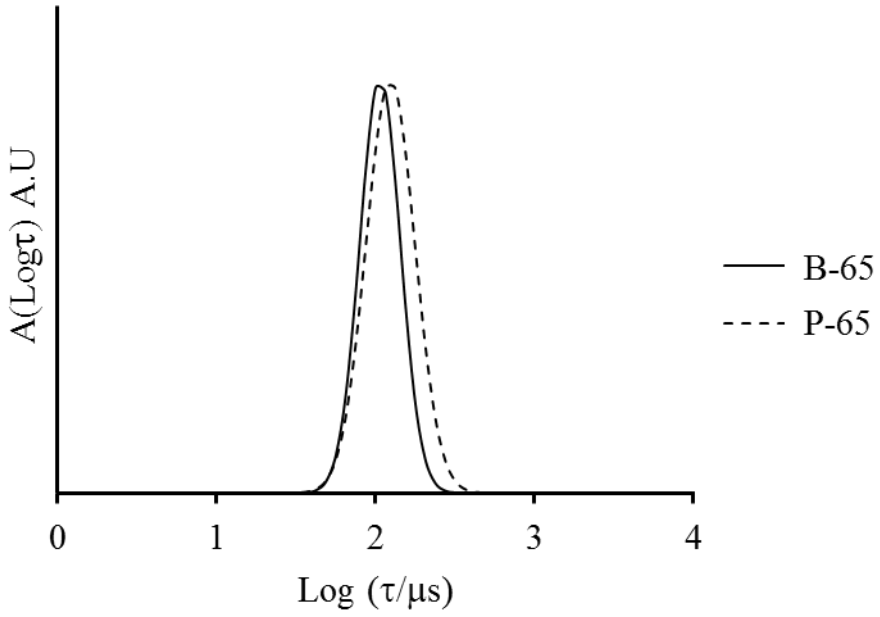

Figure S11. Relaxation time distribution of **P-65** and **B-65** at $\alpha = 0$ in 0.1 M NaCl solution, measured at $\theta = 130°$.

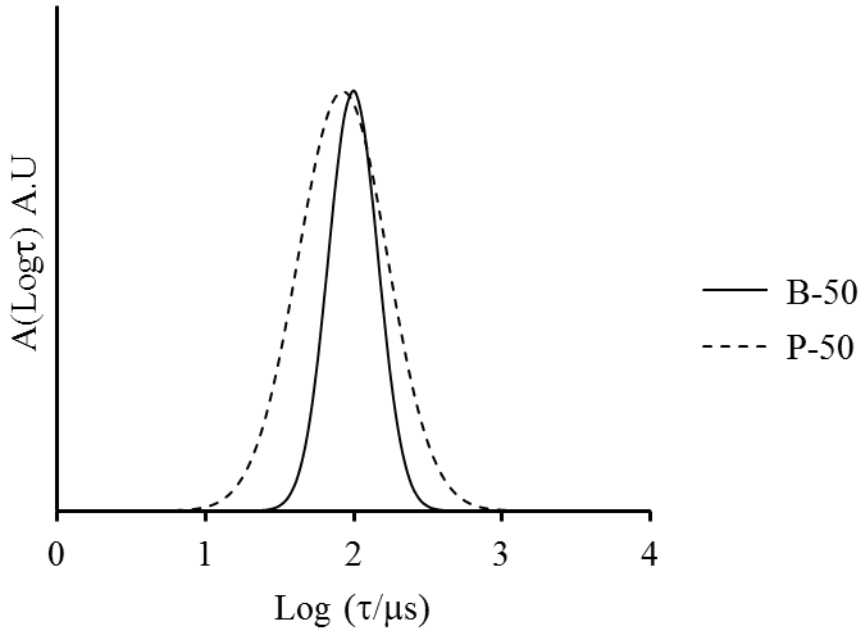

Figure S12. Relaxation time distribution of **P-50** and **B-50** at $\alpha = 0$ in 0.1 M NaCl solution, measured at $\theta = 130°$.

SAXS experiments for the P(DMAEMA-*co*-DEAEMA)-*b*-PDMAEMA diblock copolymers.

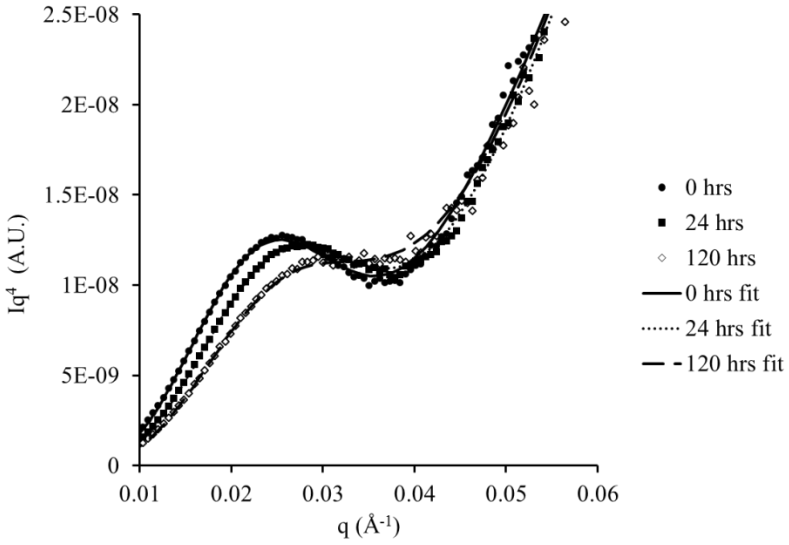

Figure S13. Porod representation of the SAXS data for **B-76** at different blending times with additional SAXS fits.

Table S6. SAXS parameters for **B-76** in Figures 2b and 2d. Values are given as provided by the software.

	0 hrs	24 hrs	120 hrs
K0	0.000125 ± 0.000145	0.00012003 ± 8.09 10^{-5}	0.00011039 ± 0.000241
K1	99.127 ± 0.148	92.597 ± 0.145	86.223 ± 0.47
K2[a]	0 ± 0	0 ± 0	0 ± 0
K3	0.21757 ± 0.00106	0.21715 ± 0.00109	0.24428 ± 0.00337
K4	8.5078 10^{-6} ± 9.77 10^{-7}	8.5797 10^{-6} ± 5.4410^{-7}	8.6461 10^{-6} ± 1.69 10^{-6}
K5[a]	8.638 10^{-5} ± 0	8.638 10^{-5} ± 0	8.638 10^{-5} ± 0
K6	1.0197 10^{-5} ± 0	1.0197 10^{-5} ± 0	1.0197 10^{-5} ± 0
K7[b]	0 ± 0	0 ± 0	0 ± 0
K8	0.0028473 ± 1.81 10^{-5}	0.0025747 ± 1.24 10^{-5}	0.0031012 ± 4.24 10^{-5}
K9	17.961 ± 0.0973	15.104 ± 0.0668	18.813 ± 0.207
K10	1 10^{-5} ± 0	1 10^{-5} ± 0	1 10^{-5} ± 0

[a] K2 and K5 are not used in this model as we only use the core part of the PCR model thus the value of thickness is set equal to zero and the value of the SLS of the shell is set to a random value. [b] One of the two background parameters has to be set equal to zero according to the NIST package for summation.

The 120 hrs' time point SAXS data is expected to be extremely similar compared to **P76**. Similar values for the core radius, the dispersity, the SLD of the core, and the thickness of the shell (parameters K1, K3, K4, and K9) are obtained thus confirming that equilibrium is reached after 120 hrs for this composition.

A decrease in the core radius (K2) is observed upon time as well as an increase of the SLD of the core (K4). Such a trend for the SLD is coherent with theoretical calculations knowing the density (determined experimentally by SLS) and chemical formula of the core (8.638 10^{-6} for a 85% DEAEMA in the core, 8.643 10^{-6} for 76%, 8.649 10^{-6} for 65%, and 8.656 10^{-6} for 55%): a decrease of % of DEAEMA in the core leads to an increase of the SLD value for the core of the micelles.

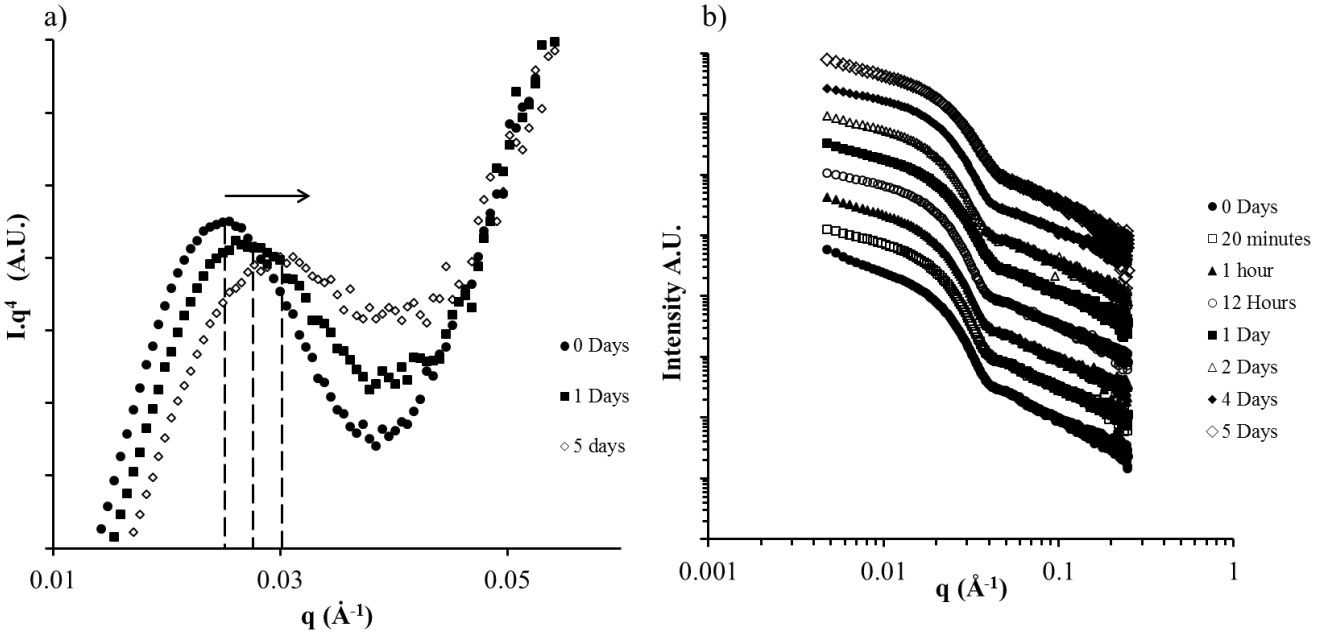

Figure S14. a) Porod representation of the SAXS data for **B-85** at different blending times, some points have been omitted for clarity. b) SAXS profiles of **B-85** at different blending times, 0 days indicates the start of the blending, using method B. Plots have been shifted vertically for clarity.

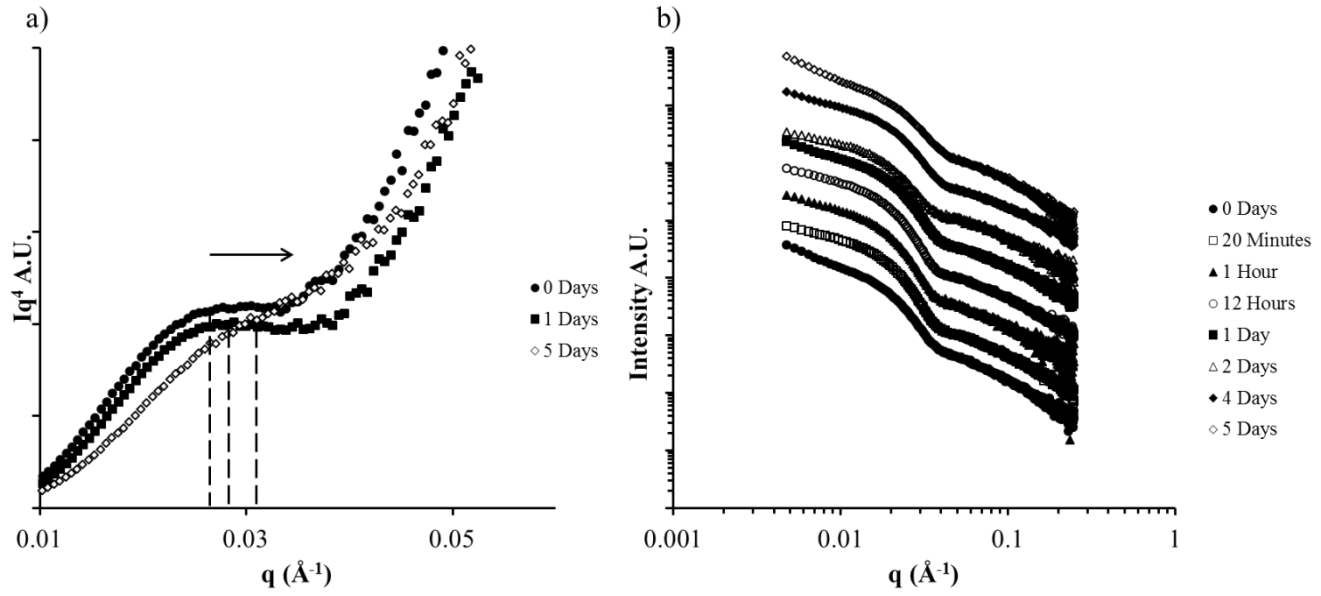

Figure S15. a) Porod representation of the SAXS data for **B-65** at different blending times, some points have been omitted for clarity. b) SAXS profiles of **B-65** at different blending times, 0 days indicates the start of the blending, using method B. Plots have been shifted vertically for clarity.

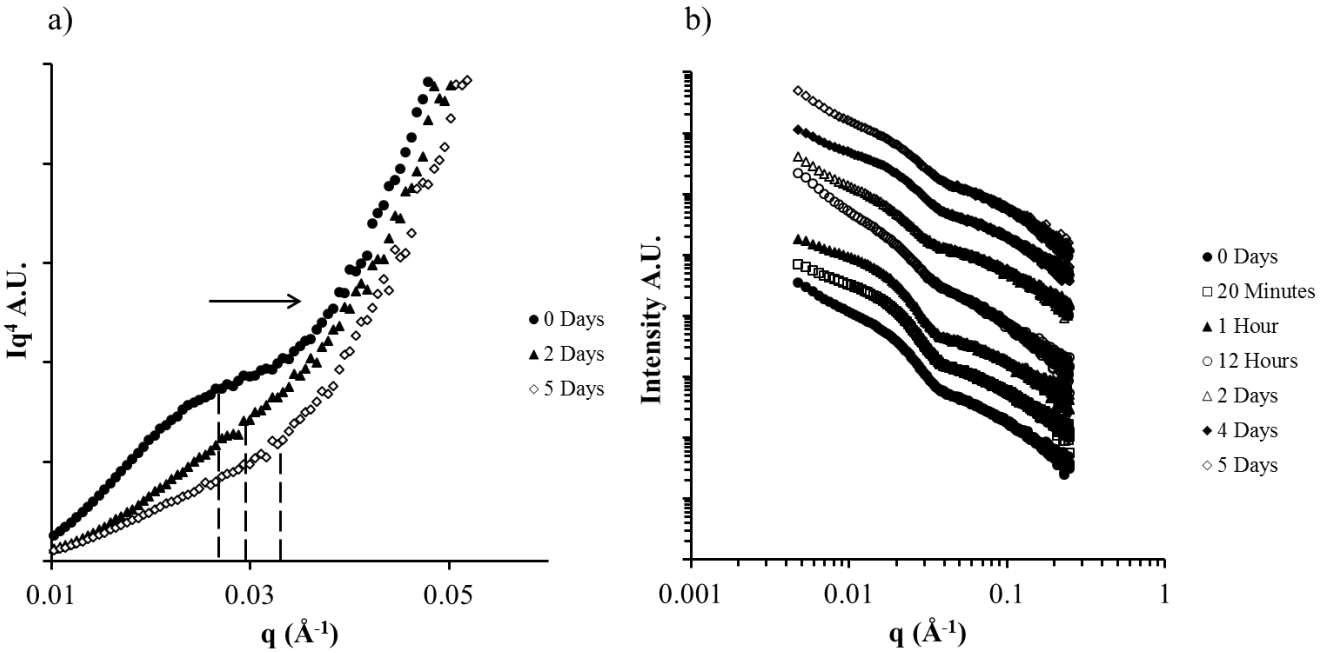

Figure S16. a) Porod representation of the SAXS data for **B-50** at different blending times, some points have been omitted for clarity. b) SAXS profiles of **B-50** at different blending times, 0 days indicates the start of the blending, using method B. Plots have been shifted vertically for clarity.

Characteristics of the P(MMA-*co*-ProMA)-*b*-PDMA diblock copolymers

Comparison of the relaxation distribution for the pure and blended micelles of P(MMA-*co*-ProMA)-*b*-PDMA diblock copolymers.

Table S7. Additional micelle scattering characterization data for all blended and pure L-proline samples in 18.2 MΩ.cm water.

	N_{agg}	$R_{h\ LLS}$ (nm)	$R_{c\ LLS}$ (nm)[a]	$R_{c\ SAXS}$ (nm)	R_{SAXS} (nm)
P-40 L-proline	9	10.2	2.5	-	-
P-25 L-proline	20	13.5	3.2	6.5	15.5
P-13 L-proline	44	11.6	4.2	-	-
B-25 L-proline	22	12.5	3.4	6.8	17.5

[a] Calculated from equation S6 assuming a core density of 1 g/L.

Table S8. SAXS parameters for P-25 L-proline and B-25 L-proline in Figure 5. Values are given as provided by the software.

	P-25 L-proline	**B-25 L-proline**
K0	0.0007888 ± 0.00167	0.0024991 ± 0.00259
K1	67.681 ± 0.229	65.316 ± 0.0811
K2[a]	0 ± 0	0 ± 0
K3	0.19098 ± 0.000744	0.19116 ± 0.000312
K4	$9.3267\ 10^{-6} \pm 9.31\ 10^{-8}$	$9.3526\ 10^{-6} \pm 3.18\ 10^{-8}$
K5[a]	$8.638\ 10^{-5} \pm 0$	$8.638\ 10^{-5} \pm 0$
K6	$9.414\ 10^{-6} \pm 0$	$9.414\ 10^{-6} \pm 0$
K7[b]	0 ± 0	0 ± 0
K8	0.0051729 ± 0.000181	0.0055046 ± 0.000327
K9	87.069 ± 1.45	111.37 ± 3.22
K10	$2.4981\ 10^{-5} \pm 5.17\ 10^{-7}$	$4.0055\ 10^{-5} \pm 5.87\ 10^{-7}$

[a] K2 and K5 are not used in this model as we only use the core part of the PCR model thus the value of thickness is set equal to zero and the value of the SLS of the shell is set to a random value. [b] One of the two background parameters has to be set equal to zero according to the NIST package for summation.

In a similar manner to equation 1 in the main text a theoretical relaxation distribution can be predicted for a non-blended mixture of micelles, as shown in equation S10.

$$A(log\tau)_{theo} = ((A(log\tau)_{13\%}.I_{13\%}) + (A(log\tau)_{40\%}.I_{40\%})) \quad \text{(S10)}$$

Where $I_{13\%}$ and $I_{40\%}$ represent the intensity of scattered light of 13% L-proline micelles and 40% L-proline micelles respectively.

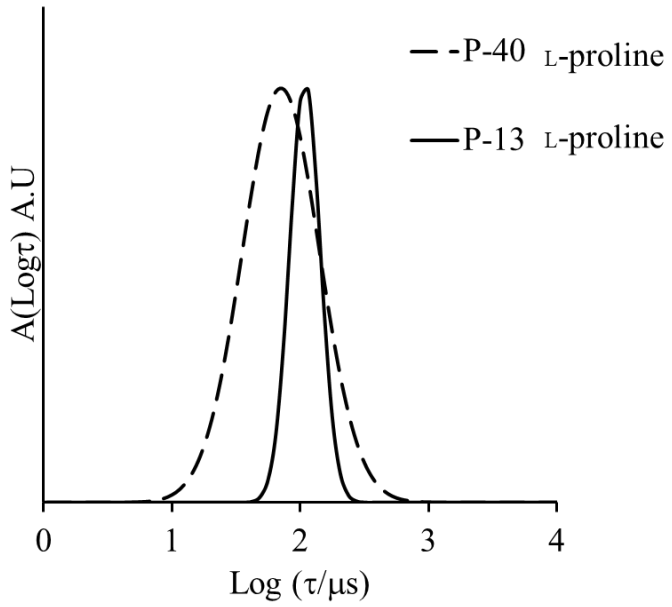

Figure S17. Relaxation time distribution of P-40 L-proline and P-13 L-proline in 18.2 MΩ.cm water, measured at $\theta = 130°$.

REFERENCES

1 Lu, A.; Cotanda, P.; Patterson, J. P.; Longbottom, D. A.; O'Reilly, R. K. *Chem. Comm.* **2012**, *48*, 9699.
2 Jakes, J. *Collect. Czech. Chem. Commun.* **1995**, *60*, 1781.

3 Nicolai, T.; Gimel, J. C.; Johnsen, R. *J. Phys. II* **1996**, *6*, 695.
4 Patterson, J. P.; Robin, M. P.; Chassenieux, C.; Colombani, O.; O'Reilly, R. K. *Chem. Soc. Rev.* **2014**, *43*, 2412.
5 Chassenieux, C.; Nicolai, T.; Durand, D. *Macromolecules* **1997**, *30*, 4952.
6 Sedlak, M. *J. Chem. Phys.* **1997**, *107*, 10805.
7 Sedlak, M. *J. Chem. Phys.* **1997**, *107*, 10799.
8 Kline, S. *J. App. Crystallogra.* **2006**, *39*, 895.
9 Glatter, O.; Kratky, O. *Small-Angle X-Ray Scattering*; Academic Press, 1982.
10 Guinier, A.; Fournet, G. *Small-angle scattering of X-rays*; John Wiley & Sons: New York, 1955.
11 Roe, R.-J. *Methods of X-ray and Neutron Scattering in Polymer Science*; Oxford University Press: New York, 2000.
12 NIST SLD calculator http://www.ncnr.nist.gov/resources/sldcalc.html.
13 NIST SLD calculator *http://www.ncnr.nist.gov/resources/sldcalc.html*.
14 Wilhelm, M.; Zhao, C. L.; Wang, Y.; Xu, R.; Winnik, M. A.; Mura, J. L.; Riess, G.; Croucher, M. D. *Macromolecules* **1991**, *24*, 1033.